

**University of Virginia Net-Zero Residence Initiative 2022 Project Energy Generation Final  
Design Report**

A Technical Report submitted to the Department of Mechanical Engineering

Presented to the Faculty of the School of Engineering and Applied Science  
University of Virginia • Charlottesville, Virginia

In Partial Fulfillment of the Requirements for the Degree  
Bachelor of Science, School of Engineering

**Jillian Doyle**

Spring, 2022.

Technical Project Team Members

Luke Anderson

Noah Plues

Joshua Starr

On my honor as a University Student, I have neither given nor received unauthorized aid on this assignment as defined by the Honor Guidelines for Thesis-Related Assignments

Harsha K. Chelliah, Department of Mechanical and Aerospace Engineering

## **Table of Contents**

<b>1. Introduction</b>	<b>1</b>
<b>2. Objectives</b>	<b>2</b>
<b>3. Background</b>	<b>2</b>
3.1 Literature Review	2
<b>4. Design</b>	<b>5</b>
4.1 Concept Development	5
4.2 Projected Performance	7
4.3 Exergy Analysis	12
4.4 Sensitivity Analysis	13
4.5 Standards and Codes	16
4.6 Prototype Design	17
<b>5. Final design</b>	<b>22</b>
5.1 Rig	22
5.2 Microelectronics and Circuitry	26
5.3 Photovoltaic System	29
<b>6. Methodology</b>	<b>33</b>
<b>7. Results</b>	<b>33</b>
7.1 Challenges	35
7.2 Comparison to Projected Data	37
<b>8. Analysis</b>	<b>38</b>
8.1 Cost analysis	39
<b>9. Future Work</b>	<b>39</b>
<b>10. Conclusion</b>	<b>41</b>
<b>11. References</b>	<b>42</b>
<b>Appendix A: Microstep Driver Additional Specifications</b>	<b>45</b>
<b>Appendix B: Arduino UNO and ATmega328P - Additional Specifications</b>	<b>50</b>
<b>Appendix C: Arduino IDE Features and Programming</b>	<b>53</b>
<b>Appendix D: Battery Instructions</b>	<b>58</b>

## 1. Introduction

With the effects of climate change becoming increasingly imminent and severe, sustainable energy generation is a crucial step to ensure a clean future. A large tool for renewable energy generation is solar energy captured by solar panels. In VA, photovoltaics (PV) is the best way to generate electricity. PV is quiet, and it takes advantage of the free, renewable energy of the sun. PV cells are most efficient when they are kept at cooler temperatures and when they directly face the incoming light. PV efficiency has improved greatly from 1%, when it was first discovered, to 8%, when it was first used in space, and now up to 40%, which means that 40% of the sun's energy striking each panel is converted into useful electricity (US DOE).

In 2016, the U.S. hit 1 M solar installations, and in 2019, we hit 2 M (Vivint Solar). Unfortunately, stationary solar panels only capture about 20% of available energy (Unbound Solar, 2015). Some of these losses are associated with factors such as heat that can be challenging to solve, but others are preventable. These losses can be decreased with a solar tracker that tilts the panel to follow the sun's path, ensuring that the panel is always perpendicular to the sun, where energy generation is most efficient. A sensor based solar tracking system was designed, with a custom rig, microelectronics, and PV set up, to compare the performance to a stationary panel.

The results of this project are aimed to be applied to the reCOVER House at Milton Airfield, that was previously built by the UVA School of Architecture. There are two simultaneous projects occurring in conjunction with the solar tracker, addressing the HVAC systems and insulation of the house. The ultimate goal is to apply these projects to make the reCOVER house an off-the-grid net-zero building. This year-long project consisted of extensive

literature review, design and testing of various tracking techniques, and finally building and testing a full scale model.

## **2. Objectives**

The main objective of this project is to create more efficient renewable energy systems while providing a hands-on learning experience for a group of senior undergraduate mechanical engineers. This project has had many iterations within the year it has been in progress, and the work is intended to continue with further groups. The long term goal is to create various solar tracking systems such as open-loop, closed-loop, and passive, to find the most efficient system. This design will then be applied to the reCOVER house, to power systems such as a heat pump.

Due to time, logistical, and monetary constraints, the goals of this year were refined to creating one working solar tracking system, that is closed-loop, from scratch, and testing the efficiency of that system compared to a stationary tracker. Unfortunately we were not able to attach the tracker to the roof of the reCOVER house, but the system is designed with that intent in the future. This system is also designed with the intent to supply power to the ground source heat pump that was also being tested for the reCOVER house, but full scale implementation has not been possible within the given time frame.

## **3. Background**

### *3.1 Literature Review*

A thorough literature review was done in the first phase of this project, which provided valuable information that shaped our design. While solar tracking systems date back to 1962, studies cite the increased efficiency anywhere from 22-56% from their stationary counterparts,

even with similarly designed systems (Seme et al, 2020; Mpodi et al, 2019). Existing trackers are split into two categories, single axis and dual axis. Single axis trackers follow the sun from east to west throughout the day, while dual axis trackers also tilt from north to south to track the sun throughout the seasons. Since this project is being constrained to single-axis systems with various passive and active systems, similar existing systems were analyzed.

The design of the passive tracker is largely based on the work done by Clifford et al. (2003) with the novel design of utilizing the expansion properties of bimetallic strips. The bimetallic strips were made of aluminum and steel and attached to either side of the solar panel. The strips were connected to the panel frame on each end with a mass sitting in the middle of the strip. Shades were attached to the outside of each strip to control which angles the sunlight hit the metal strip. The prototype created by Clifford et al. is shown in Figure 1 below.



Figure 1: Passive tracker design utilizing two bimetallic strips by Clifford et. al.

As the sun hits the exposed bimetallic strip, the aluminum and steel expand at different rates, causing the strip to bend. The strip is arranged so it bends away from the sunlight and the mass difference causes the panel to rotate. This means that the Aluminum is on the bottom side

of the strip, and the steel is layered on top. Figure 2 below shows a side view of the strip in a neutral position and when heated. This passive design is the same that will be explored throughout this project.

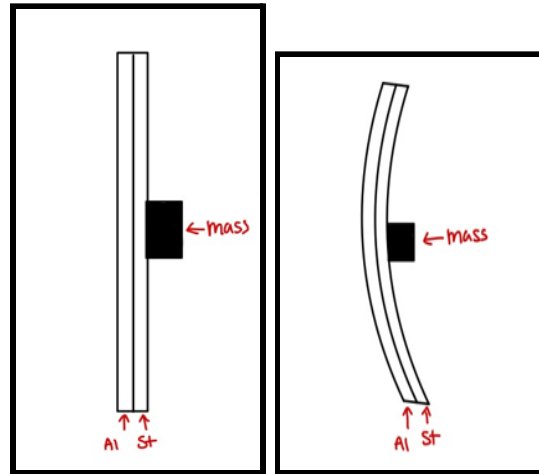


Figure 2: Bimetallic strip design shown in a neutral position (left) and when heated (right).

Active trackers are much more popular in industry. A research paper by Chowdhury et al. details the popular designs of active trackers as well as the development of an algorithm for an open-loop system. The design of these two systems are shown in figure 3 below, but are for dual axis trackers whose range of motion has two degrees of freedom.

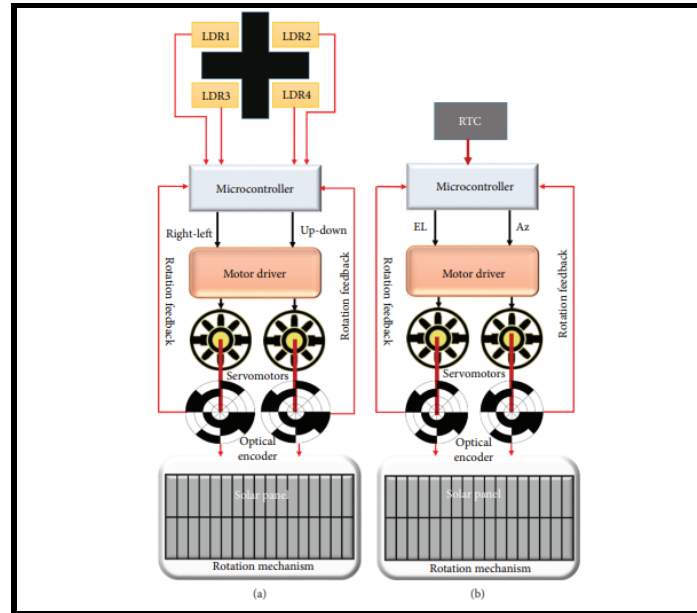


Figure 3: System block diagram (a) using optical tracking and (b) using proposed sun position algorithm based tracking.

The closed loop tracker (a) uses photoresistors to determine where the sun is, then moves the panel accordingly. The open loop tracker (b) uses a pre-programmed algorithm instead of sensors to determine where the sun is in the sky based on the time of day and location of the tracker. This paper concluded that the open loop tracker performed better than the closed loop tracker.

## 4. Design

### 4.1 Concept Development

Originally this project was designed to compare all three tracking systems; passive, open-loop, and closed-loop, to determine which was the most effective. All three systems were designed on the theoretical level, but early on it became clear that the passive tracking system was not feasible to scale up. This was due to both a lack of documentation on the creation of

these systems as well as a lack of materials and skills such as bimetallic strips and working with pressurized tubes with chemicals.

The active tracker design became the most obvious choice to pursue as it combined the application of various engineering techniques learned throughout the undergraduate mechanical engineering curriculum. The closed-loop sensor based tracking system was chosen as the first to build as the open-loop design could be easily added on in future work.

The overall design adhered to various technical and logistical constraints. To adhere to the requirements of the capstone design project as a whole, the integration of knowledge built throughout the mechanical engineering undergrad curriculum with the application of an original design were considered. The design should offer some additional innovations on pre-existing designs by making the rigs as compact and simplistic as possible. For this, the rig should be a single axis tracker that conforms closely to the roof, up to around 30 deg tilt above the horizon. Having a single axis design means that the rotation of the rig would be limited to around 30 deg from the zenith and would not account for daily the changing altitude of the sun. Future designs should be examined for practicality like having minor adjustments of the from horizon angle of the tracker every month.

The system was designed with the intent of rooftop installation on the reCOVER House at Milton Airfield, shown in figure 4 below. The roof is approximately 800 sq ft. titled at  $7.125^\circ$  directly south.



Figure 4: The reCOVER House at Milton Airfield (left) and the architecture drawings (right).

### 4.2 Projected Performance

Since the operating temperature of the solar array is not controllable, the only way to increase its efficiency is by pointing each panel directly at the Sun. Earth is constantly bombarded by  $\sim 1,400 \text{ W/m}^2$  of perpendicular solar flux. Some of that sunlight gets reflected back into space. After scattering due to atmospheric effects, only a portion of the original solar radiation makes it to Earth's surface. Cloudy weather increases the scattering effect, producing more diffuse radiation. Ignoring the diffuse radiation, a dual-axis solar tracking surface would receive what is called direct normal irradiance, or DNI.

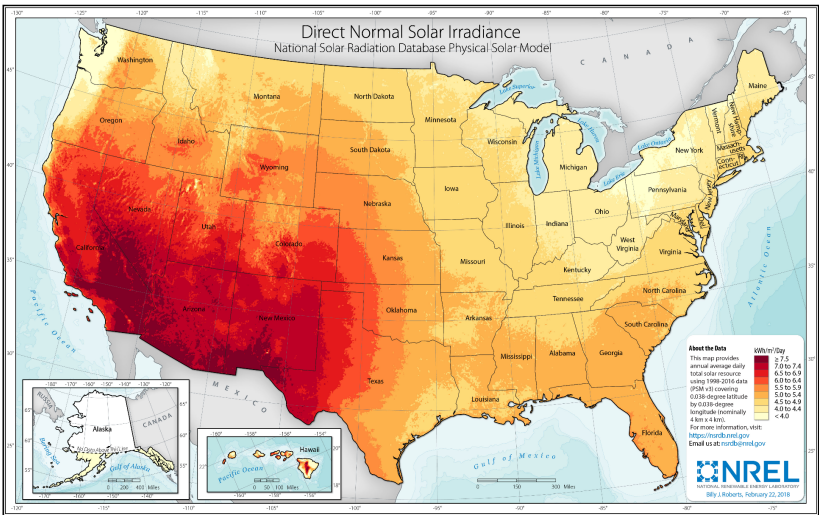


Figure 5: The annual average amount of DNI in the U.S.

DNI data can approximate the amount of solar radiation a single-axis solar tracking surface would receive. A horizontal stationary surface receives what is called global horizontal irradiance, GHI.

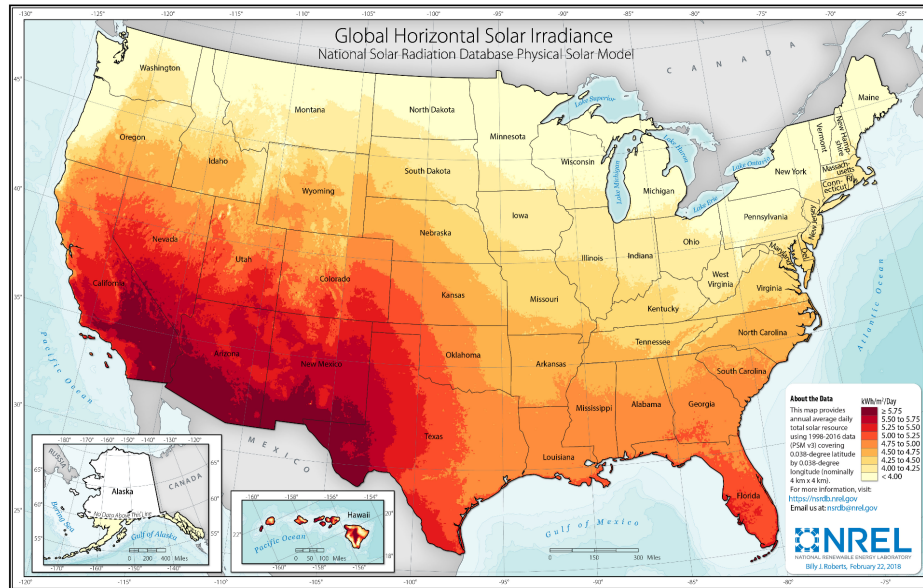


Figure 6: The annual average amount of GHI in the U.S.

When compare the annual DNI and GHI in Charlottesville, VA, it can be seen that a horizontal stationary solar panel receives  $\sim 4.5$  kWh/m<sup>2</sup>/Day while a solar tracking panel receives  $\sim 5$  kWh/m<sup>2</sup>/Day, resulting in an 11% increase in efficiency year-round. Because DNI does not include diffuse radiation, which can be significant in cloudy areas, 11% may be a low estimate, especially in Virginia.

The local coordinates of objects in the sky are shown in figure 7 with zenith pointing straight up from the observer and the altitude being the angle from the horizon while the azimuth is the angle from direct south following a clockwise direction.

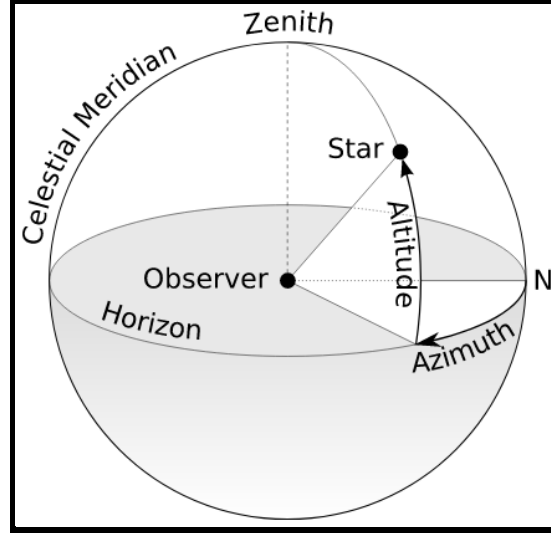


Figure 7: Various global angles used to develop tracker algorithm.

The first calculation needed is the local hour angle (degrees) based on local standard time.

$$h = 15(LST - 12) \quad (1)$$

Next, the number of days since new year ( $d$ ) is used to get the declination of the sun at the current day. This is the angle in degrees the sun is from the equator.

$$\delta = 23.45 * \sin\left(\frac{2*\pi(d+284)}{365}\right) \quad (2)$$

The declination angle ( $\delta$ ) and local hour angle ( $h$ ), with the latitude the tracker known to be 36 degrees from the equator ( $L$ ) allows for the solving for the altitude of the sun.

$$\alpha = \arcsin(\sin(L)\sin(\delta) + \cos(L)\cos(\delta)\cos(h)) \quad (3)$$

The above equations solve for the altitude of the sun at a day and time. To solve for the azimuth of the sun the declination angle the altitude ( $\alpha$ ) and the local latitude ( $L$ ). The angles need to be converted to radians for the solar azimuth angle calculations.

$$\gamma = \arccos\left[\frac{\sin(\alpha)\sin(L)-\sin(\delta)}{\cos(\alpha)\cos(L)}\right] \quad (4)$$

To further predict the improvement of a solar tracker PV system over a stationary one, some calculations to determine the irradiance differences between the two cases. Using the sun position equations gathered early, using equations 2, 3, and 4, the panel irradiance (I) could be found using an equation given by Veligorskyi (2014) with the panel tilt (0-90 degrees) from the horizon, the altitude of the sun, azimuth of the sun from the south, and azimuth of the panels from the south, where  $I_G$  is the ideal direct sunlight irradiance. The irradiance is graphed in figure 8 on the next page.

$$I = I_G(\cos(\alpha)\sin(\beta)\cos(\psi - \gamma) + \sin(\alpha)\cos(\beta)) \quad (5)$$

To use equation 5 the ideal direct irradiance would be needed to be found. This could be done by approximating the irradiance. The irradiation in  $\text{kW/m}^2$  could be found with AM, air mass (eq. 24), 70% radiation incident from the earth's atmosphere, and the solar constant of  $1.353 \text{ kW/m}^2$  (Honsberg and Bowden, 2021).

$$I_G = 1.1 * 1.353 * 0.7^{AM^{0.678}} \quad (6)$$

With AM being dependent on the azimuth of the sun altitude and using the sun location equation.

The Energy production in kWh is determined by eq. 7.

$$E = P_{nom} / (I_{nom} T_{day}) \int_0^{T_{day}} I(t) dt \quad (7)$$

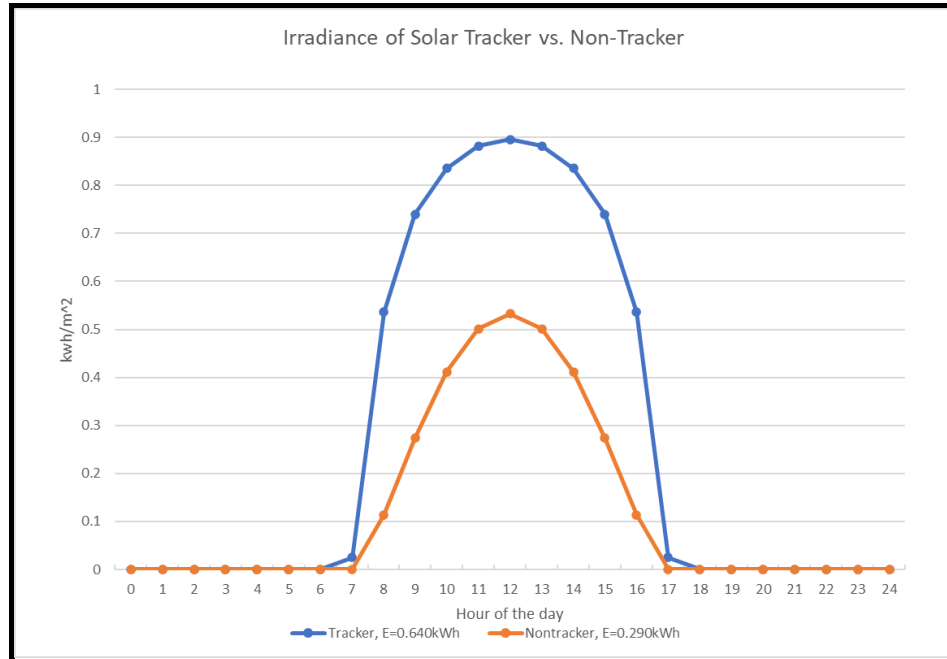


Figure 8: The predicted irradiance of a full solar tracker vs a flat solar panel facing directly at zenith. The irradiance is showing the rough estimate of the radiation each case would yield using equations from Veligorskyi paper (p. 4, 2014) and Honsberg and Bowden (2021).

The data above in figure 8 is modeling the non-tracking system under the ‘worst-case scenario,’ where the panels would be facing straight up to the zenith. The active tracking curve is assuming a full 2-axis tracking system with 90 degrees of motion. This graph shows that most of the radiation that the panels will receive would occur at the peak hours of the day. The last couple hours of the day also provide very little radiation. The sunlight loses a lot of energy at dusk and dawn hours due to having to pass through a high amount of the atmosphere to get to the observer. This makes the light reflect and refract so that some spectrums of light are scattered. This data suggests that only the peak 4-6 hours of the day need to be used to collect energy from the sun, while the energy produced at the low hours is largely not worth collecting. The data also shows that a solar tracker could increase energy production to up to around 200%. With the total kWh of the tracker being greater than the non-tracker. The area under the curves of the Irradiance

is the energy, with 0.640kWh for the full tracker, and 0.290kWh for the flat (facing direct zenith) non-tracker.

### 4.3 Exergy Analysis

Exergy is defined as the amount of energy a system can perform along a reversible process when it is brought into thermodynamic equilibrium with its environment (Jørgenson, 2008). When accounting for the number of moles and chemical potential energy of each species that makes up the system, the equation for specific exergy expressed below can be found (Regalbuto, 2014). The subscripted terms represent various state variables at the dead state, where the system is presumed to be unable to generate any work.

$$\phi = u - u_0 + P_0(v - v_0) + T_0(s - s_0) + \sum_i y_i \mu_{i,0} \quad (8)$$

The exergetic efficiency of a photovoltaic solar cell is given by:

$$\eta_{ex} = \frac{\mathbf{E}_{out}}{\mathbf{E}_{in}} = \frac{\mathbf{E}_{elec} - \mathbf{E}_{thermal-losses}}{\mathbf{E}_{solar}} \quad (9)$$

Where  $\mathbf{E}_{elec}$  is the electrical exergy,  $\mathbf{E}_{thermal-losses}$  is the exergy of thermal losses, and  $\mathbf{E}_{solar}$  is the solar exergy. When accounting for the expressions for these three terms, the equation is:

$$\eta_{ex} = \frac{V_m I_m - \left(1 - \frac{T_0}{T_{cell}}\right) h A (T_{cell} - T_0)}{\left(1 - \frac{T_0}{T}\right) A I} \quad (10)$$

Where  $V_m$  and  $I_m$  are the maximum voltage and current of the solar panel,  $T_0$  and  $T_{cell}$  are the temperatures of the atmosphere and the solar cell, and  $h$ ,  $A$ , and  $I$  are the convective heat transfer coefficient, the area of the solar panel, and the incoming solar irradiation, respectively.

Note that the convective heat transfer coefficient,  $h$ , has a linear relationship with the wind velocity,  $v$ , as  $h = 5.7 + 3.8v$  (Moran et. al, 2018).

#### 4.4 Sensitivity Analysis

Sensitivity Analysis, by definition, is the study of how the uncertainty in the output of a model can be attributed to the uncertainty of any one model input (Saltelli).

$$Sensitivity = \frac{Input_0}{Output_0} * \left( \frac{d(Output)}{d(Input)} \right) \quad (11)$$

The output that is most relevant is the exergetic efficiency, which depends on numerous environmental factors and is important due to exergy being the amount of useful work transferred to the system. The sensitivity of the exergetic efficiency will be calculated with respect to the atmospheric temperature, the time of the day, and the specific date within the year. The reason why it would be of interest to take the date and time into account is because they both factor into  $\alpha$ , the elevation angle, as well as  $\delta$ , the declination angle. In addition, since there is no reliable way of measuring the temperature of the solar cell, it is safe to assume that the cell's temperature is the same as the ambient temperature. Although it is possible to perform a

sensitivity analysis with the wind speed as the input variable, doing so would entail the removal of this assumption. Because the solar panel is designed to track the movement of the sun using an active mechanism, the azimuth angle of the panel would be the azimuth angle of the sun. Therefore, our final equation for exergetic efficiency is:

$$\eta_{ex} = \frac{V_m * I_m}{(1 - \frac{T_0}{T_{sun}}) * A * I_G * [\cos(\alpha) * \sin(1 - \alpha) + \sin(\alpha) * \cos(1 - \alpha)]} \quad (12)$$

where the solar irradiance at the Earth's surface at a plane perpendicular to radiation,  $I_G$ , is given by equation 6, and the correction factor, AM, is expressed as:

$$AM = \frac{1}{[\cos(\theta) + 0.50572 * (96.07995 - \theta)^{-1.6364}]} \quad (13)$$

And the angle between the normal of the surface and the position of the sun  $\theta$ , is expressed as using the altitude of the sun from equation 14:

$$\theta = 90^\circ - \alpha \quad (14)$$

Calculating the derivative of  $\eta_{ex}$  with respect to  $\alpha$  would be extremely tedious and cumbersome. Instead default values of each input variable will be given as LST = 12,  $d = 172.25$  and  $T_0 = 303.15$  K. In other words, the default state will be at midday, on the summer solstice, at 30 °C. The reason for setting this set of parameters as the default state is because at noon during the summer solstice, the incremental change in exergetic efficiency is expected to be zero.

Conversely, the spring equinox at daybreak will be used to highlight the opposite case, as the sensitivity is expected to be at its peak. Here, LST = 7,  $d = 79.25$ , and  $T_0 = 283.15$  K. All temperature perturbations will be 1K, all perturbations of LST will be 1 hour, and all perturbations in  $d$  will be 1 day.

Assuming the default state,  $h = 0$ ,  $\delta = 23.45^\circ$ , and  $L = 36^\circ$  from the horizontal,  $\alpha$  is  $77.45^\circ$ . From there,  $\theta$  equals  $0^\circ$ , which is expected at noon, no matter what day it is. Because  $\theta = 0$ , the correction factor AM is 1.024. Irradiance =  $1.036 \text{ kW/m}^2$ . The prototype has dimensions of  $0.2\text{m} \times 0.25\text{m}$  and optimum operating voltage and current of 18V and 0.27A, respectively. Using these parameters, the exergetic efficiency of the prototype at  $30^\circ\text{C}$ , at 12:00 PM during the summer solstice is 11.771%. If the LST is perturbed by 1 hour such that the exergetic efficiency is measured at 1:00 PM, the exergetic efficiency is 11.848%. The sensitivity of exergetic efficiency to the sun's position in the sky is:

$$S_{Hour} = \frac{12}{0.117705770241} * \frac{0.118483346878 - 0.117705770241}{13 - 12} = 0.079273255890 \quad (15)$$

Using the same process, the sensitivities of exergetic efficiency to the day of the year and the temperature can be expressed as follows:

$$S_{Day} = \frac{172.25}{0.11771} * \frac{0.117706164979 - 0.117705770241}{173.25 - 172.25} = 0.000577657496 \quad (16)$$

$$S_{Temp} = \frac{303.15}{0.117705770241} * \frac{0.118504996174 - 0.117705770241}{304.15 - 303.15} = 2.05839816598 \quad (17)$$

At the state where sensitivity is expected to be at its highest, the equations above can be expressed as follows:

$$S_{Hour} = \frac{7}{0.230516665346} * \frac{0.15936745018 - 0.230516665346}{8-7} = - 2.16055748253 \quad (18)$$

$$S_{Day} = \frac{79.25}{0.230516665346} * \frac{0.22757704965 - 0.230516665346}{80.25-79.25} = - 1.01061909584 \quad (19)$$

$$S_{Temp} = \frac{283.15}{0.230516665346} * \frac{0.230558632024 - 0.230516665346}{284.15-283.15} = 0.014427847230 \quad (20)$$

Surprisingly, while the sensitivity to changes in date and time dramatically increased during the morning and evening, as well as during spring and autumn months, sensitivity to changes in temperature saw the opposite trend.

#### *4.5 Standards and Codes*

The overall goal is to design and build a stand-alone, battery-based solar tracking system capable of being mounted onto a residential roof. Safety is our top priority for this project. The rooftop system will be made from many parts (e.g., panels, controllers, and inverters), and the group carefully followed all instructions that come with these components and were assisted by a certified electrician. The National Electric Code (NEC) has been adopted by Virginia to ensure public safety regarding electrical projects. The following standards from Article 690 are required for photovoltaic (PV) solar installations in the US:

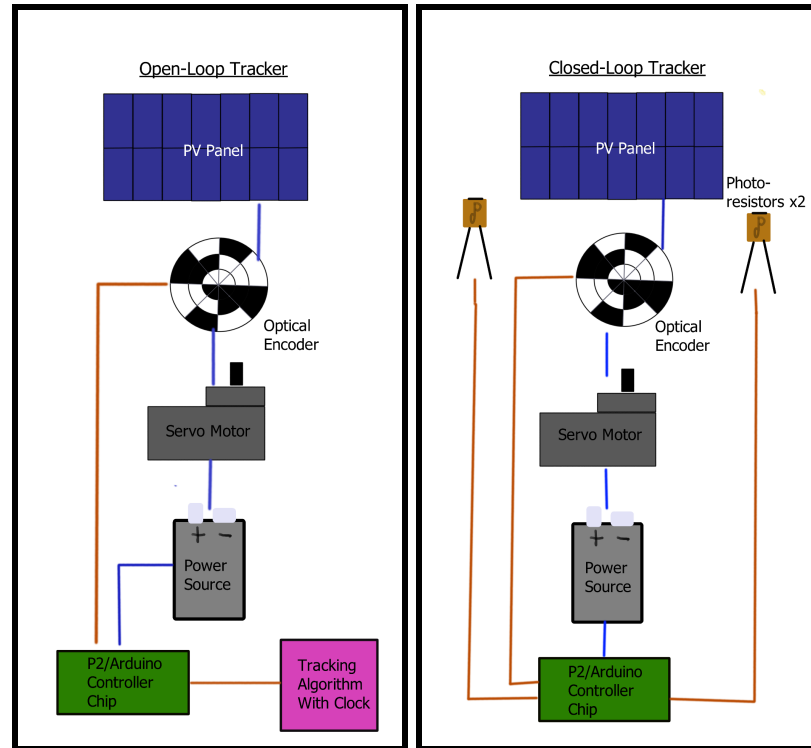
- A maximum voltage of 600 V for a single-family dwelling

- A rapid shutdown function for rooftop systems that can be accessed from outside the building
- Specific warning labels on all wires and disconnects

These factors were all considered in the implementation of our design, and should remain a priority as the project is expanded into rooftop installation.

#### *4.6 Prototype Design*

The first step for developing the rigs consisted of understanding the major components of the rig and how they interact with each other as shown in the figure below. The majority of the active trackers consist of a tracking algorithm or set of photoresistors that relay data to the microcontroller. The microcontroller then enables the power supplies to give the servo motor current to drive it a certain amount of steps. In turn, making the pc panel rotate on one axis across allows it to follow the sun across the sky.



(a)

(b)

Figure 9: Flow charts for (a) the open loop tracker and (b) the closed loop tracker.

The rigs for all of the tracking systems were kept as similar in design as possible to limit complexities in testing. Below is a two-dimensional sketch of the general rig design first envisioned. The design was made to be as compact as possible to improve appeal on the installation of the final design on domestic roofs.

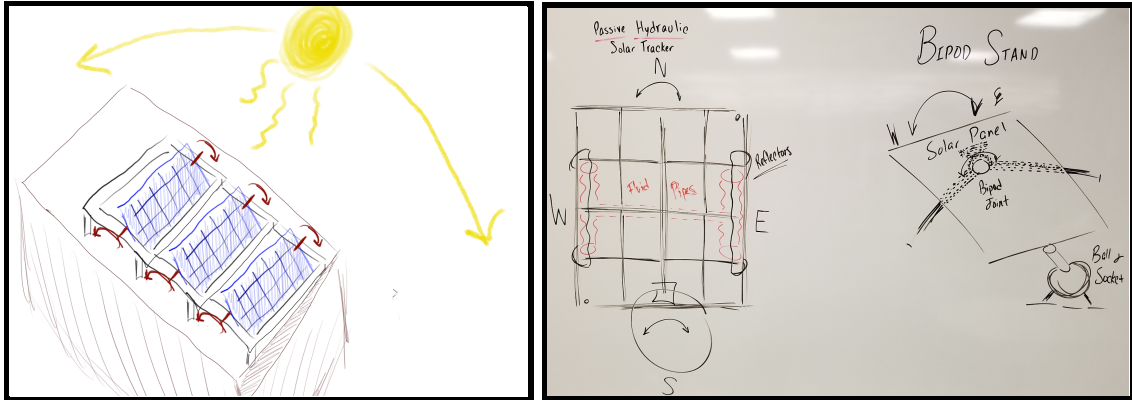


Figure 10: The (a) conceptual vision of the Rigs on the roof and (b) more detailed ideas for the design.

With the approval of the basic model idea, 3d designs were developed of the prototyping rigs to fit a finalized 8''x10'' solar panel on a tray that will rotate on a single pivoted axis at a 40 degrees angle. First designs had a bipod attached to the back of the tray but it was determined the bipod offered little structural benefits and took away from the ascetics of a sleek design.

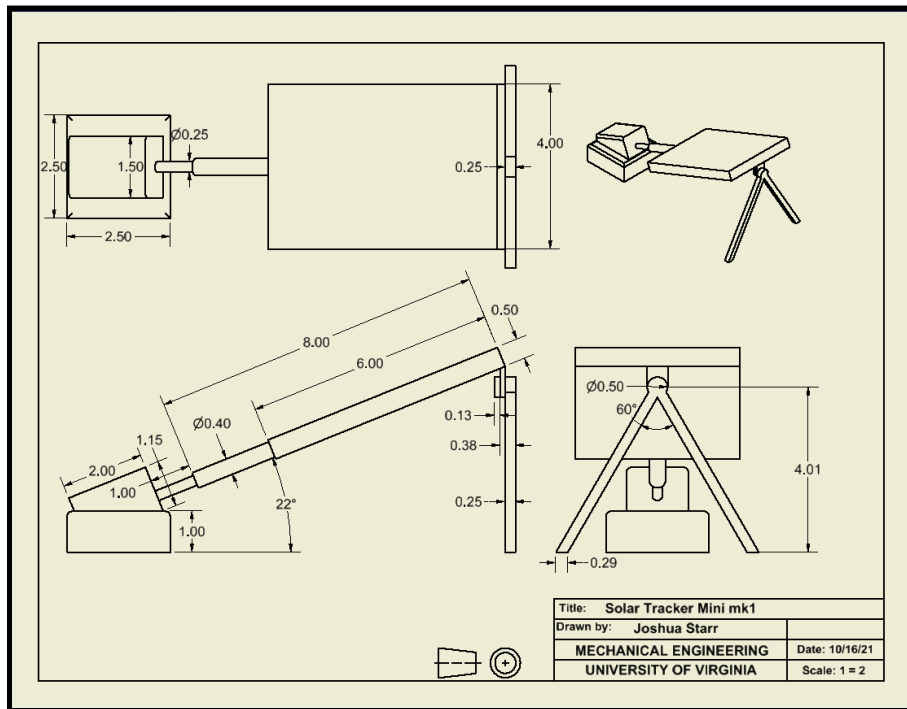


Figure 11: The first 3D model design for the rig, this design included a bipod for extra support and a tray size designed to fit a 4''x6'' solar panel.

The final prototype design had three universal parts across all tracker types. The first is the base which has mounting points for the rig to attach to the ground as well as space to attach a stepper motor. The design also has a clamp that connects to the base either directly with the passive design or indirectly with the stepper motor. The last structural component is the tray, which will be an 11/32" thick piece of plywood screwed to the clamp, for the prototype, as shown in figure 12 below. For the closed-loop tracker a small photoresistor mount could be attached to the clamp.

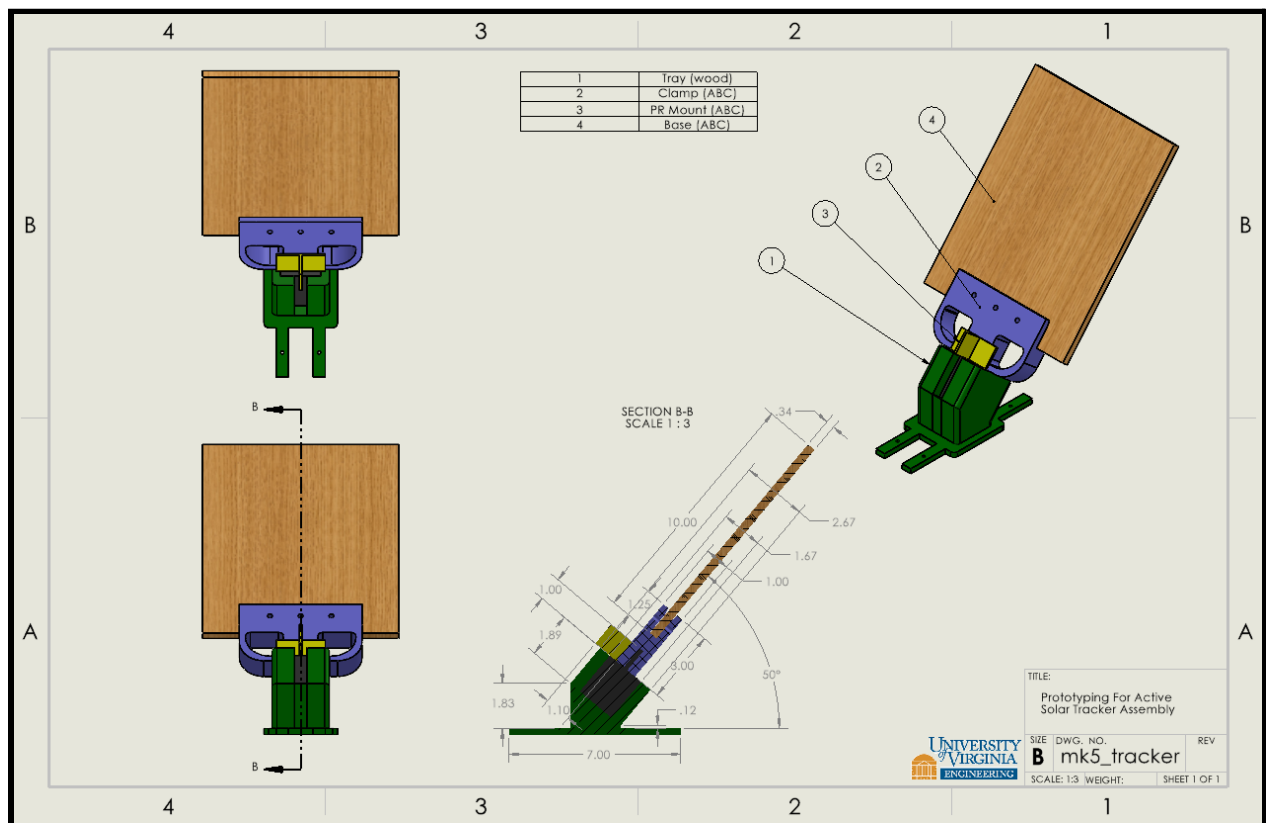


Figure 12: Drawing of mk5 active tracker prototype. This was the final prototype design made.

Due to issues ordering parts and time limitations only one active tracker (closed-loop) was fully assembled. The tracker is mounted to a wood platform to allow for a sturdy and portable fixture point.

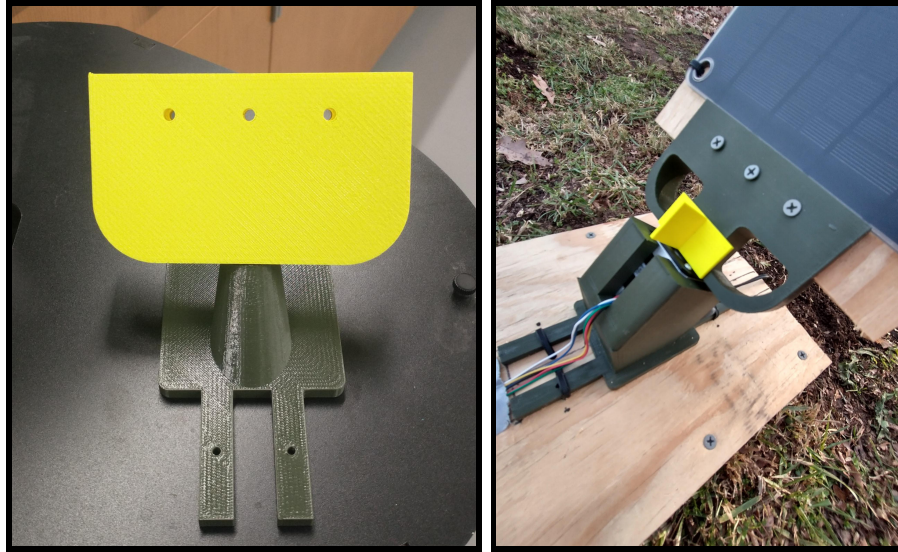


Figure 13: A mk5 printed in ABS plastic passive tracker on 11/16/2021 without the damper or tray on the left. A printed ABS active tracker that is fully assembled on the right.

For the microelectronics for the prototype it was concluded that the project should use a stepper motor. This allows for an accurate linear movement of the solar panel when tracking. The stepper will need a button/sensor to locate home during reset and know when the motor has rotated to its limit. The prototype uses a 6-lead unipolar/bipolar stepper motor, 200 steps/rev, 42×48mm, 4V, 1.2 A/phase (Pololu Robotic & Electronics, 2021). This motor has a holding torque of around 3.2kg-cm and has steps of 1.8 degrees. The motor was mounted in the base of the active tracker with help of a Pololu bought NEMA 17 aluminum mount.

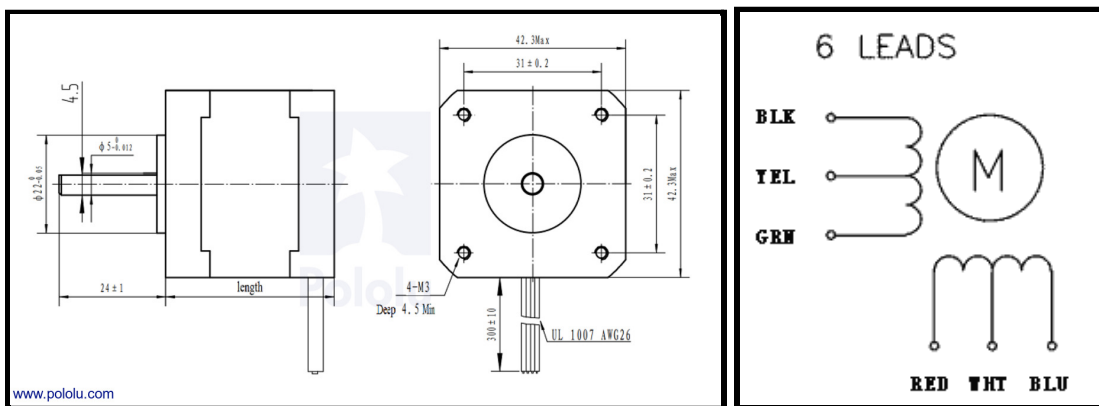


Figure 14: Dimension of the 42x48mm stepper motor (in metric mm) on the left. 6-leads wiring diagram for the stepper motor on the right (Pololu, 2021).

## 5. Final design

### 5.1 Rig

The rig consists of the panel, frame, bipod, base, and mount functions mainly to provide structural integrity to the solar panels within a system that can rotate with the motor.

Quantitatively, we wanted a sleek, aesthetically pleasing rig that could potentially be attached to a rooftop without being too heavy or tall. It appeared that all existing designs were meant to stand alone away from a structure, so this was a key differentiating factor with the overall design. Additionally, consideration factors included the panel's angle and range of motion, motor torque, back driving, weight, fixtures and attachments, and weathering.

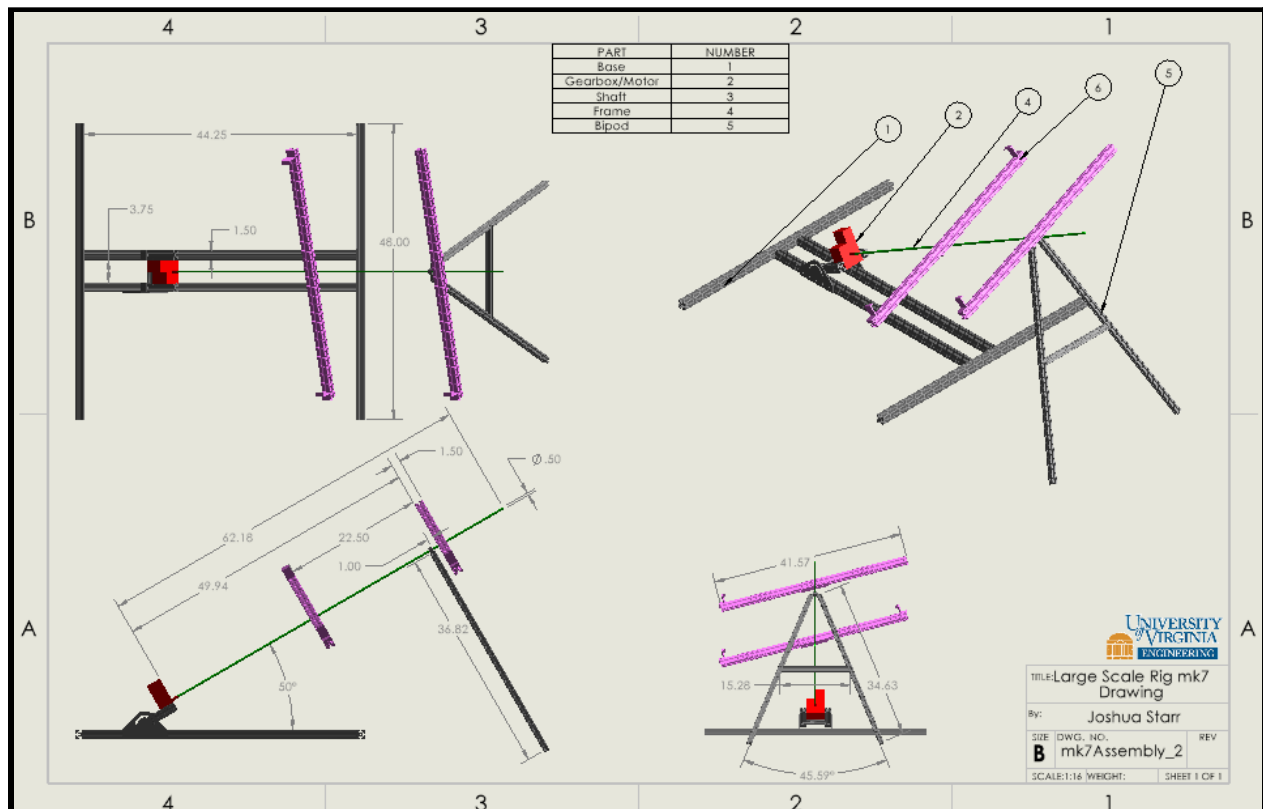


Figure 15: Final rig engineering drawing.

The rig has a single axis movement of  $\pm 45^\circ$  yaw and a semi-adjustable pitch fixed for  $50^\circ$  from the horizon. A worm gear with a 1:30 ratio addressed the concerns of torque and back driving. The gear ratio helped amplify the motor's torque so it could move the weight of the panel, and worm gears can not be back driven, so there was no concern of the panel moving the motor. The rig rotates via a long steel shaft (1/2" DIA) that connects directly to the gear shaft via a bored clamp. The gear connects to the motor shaft, as shown in figure 16.

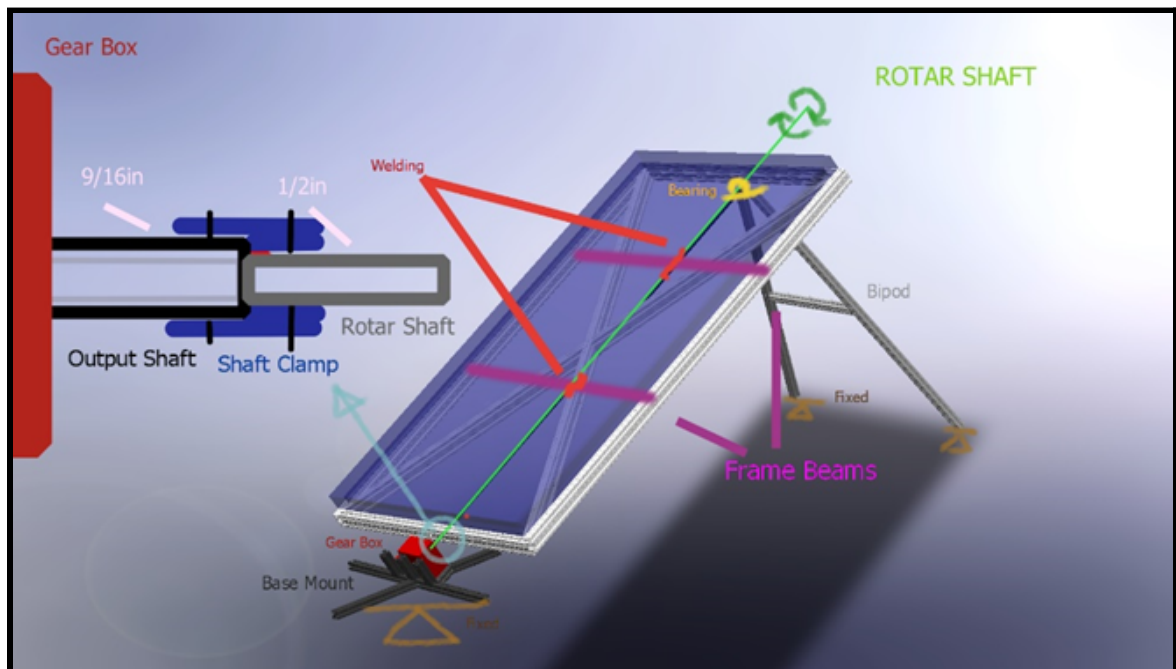


Figure 16: Final rig 3D rendering with motor schematic.



Figure 17: Images showing some key parts of the final rig: the extrudable part of the base (top left), the welding of the shaft (top right), the adjustable mount (bottom left) and the shaft coupling (bottom right).

The panel is held up by a supportive aluminum frame that is bolted to a steel plate; the steel plate has been welded to the shaft. The shaft is supported at one end by a gearbox bearing and at the other end by the bipod bearing. The base and mount design is also aluminum. The specifications of the base changed many times; issues with how to mount the gearbox to the base while still offering good support and stability for the rig. Most of the rig is aluminum due to its weight-strength combinations and corrosion resistance. All beams in the design are 20/20 extruded aluminum with a 1.5” width and are bolted together. The final rig components are shown in figure 18 below.

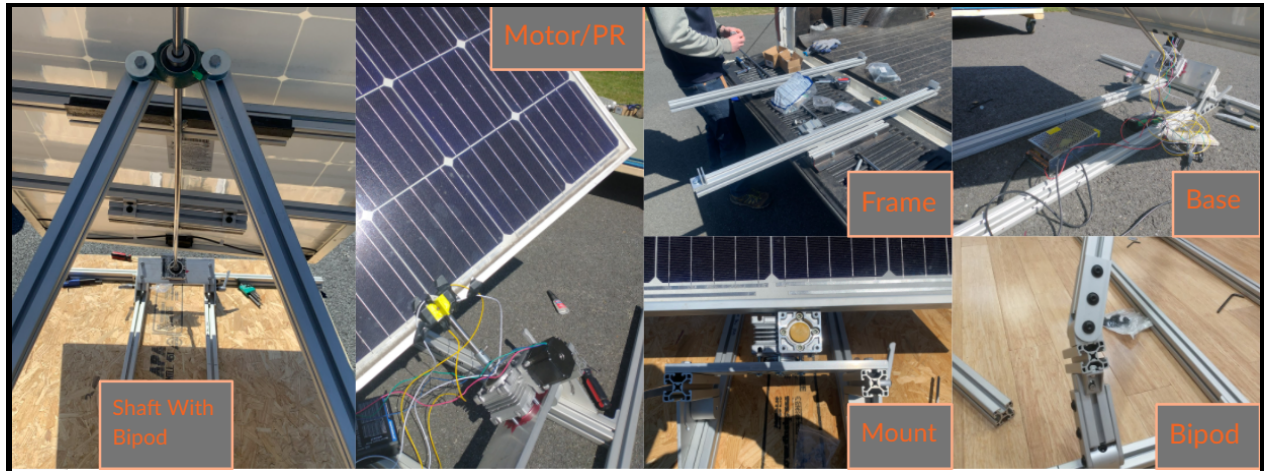


Figure 18: Images Showing the shaft, motor, mount, frame, bipod and base for the final rig.

The final rig had some last additions. The rig was altered to be semi-adjustable in its angle, with the bipod, base, and monitor positions can be adjusted. The bipod has two hinges that give it two axes of rotation (figure 18). The base can also be extended and contracted (figure 17). Lastly, the motor mount angle can be changed (figure 18). Figure 19 shows the final assembled rig, it has a sturdy base, frame, and bipod design that is still lightweight enough to only need two people to carry even with the panel on.



Figure 19: Image of the rig wired and running during the first day of testing.

## 5.2 Microelectronics and Circuitry

An electronic system made of many components was employed to direct and control the rig's dynamic capabilities, both automatic and manual. The five main parts of this system were the power supply, the driver, the motor, the microcontroller board, and the collection of small electrical components that performed various functions based on the command of the microcontroller.

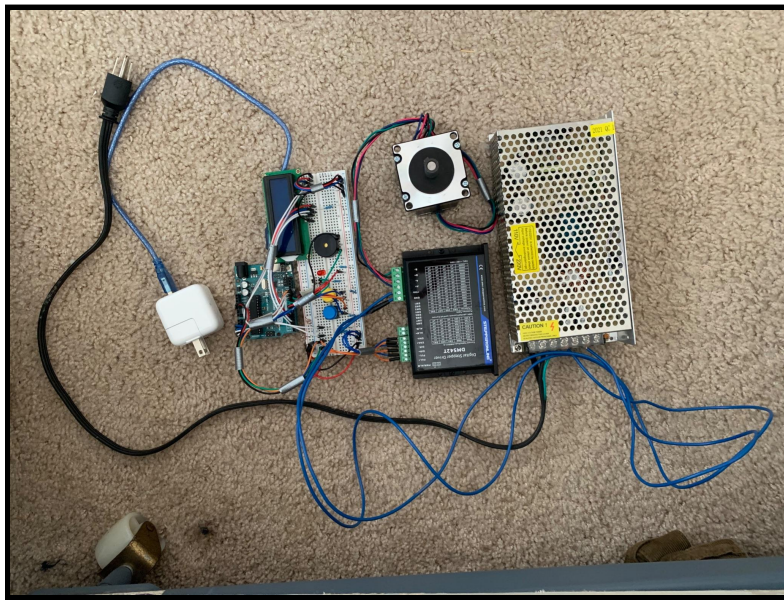


Figure 20: Full Layout of the Microelectronic System.

The power supply is a 24V power supply that has an aluminum frame and has ports that connect to the hot, neutral, and ground wires of an NMB cable to be plugged into a common 3-prong plug to be found in commercial and residential buildings. Other ports include three positive and three negative terminals, of which one of each was to serve as the source of power for the stepper driver (Lowe).

The stepper driver was a DM542T 2-phase digital stepper drive with microstepping capabilities. The particular version of the driver that was used was the fourth revision, finalized in October 2020, which added a 5V/24V logical voltage selector and alarm outputs (DM54t

Datasheet). The current that the driver is able to output ranges from a minimum of 1.0A (0.7 RMS) to a maximum of 4.5A (3.2 RMS), while the range of DC voltages that it is able to supply has a minimum of 18V and a maximum of 50V, with the typical range being 24-48V. The maximum pulse input frequency is 200 kHz. Additional specifications for the driver can be found in Appendix A.

Although a variety of motors could have been controlled with the system, special considerations had to have been made to account for the motor size, the shaft diameter, the maximum current per coil, and the holding torque. Testing was first performed on a variety of motors and drivers, including the 28BYJ-48 and ULN2003, as well as various NEMA-17 unipolar and bipolar motors with the DRV8825. However, due to the low holding torques of these motors, they were relegated to be for testing purposes only (28BYJ-48 DataSheet, 17HS16-2004s Datasheet).

The motor that was used to operate the final design was a hybrid NEMA-23 stepper motor with a holding torque of 12 N-m, an input voltage of 3V, a rated current per phase of 2.8A, and a shaft diameter of 6.35 +/- 0.013 mm, which was of particular importance in order to ensure that the key that came with the gearbox was able to house the motor without any issues (24V NEMA 23 Data Sheet). The wires that ended up corresponding to the A+, A-, B+, and B- terminals were colored blue, red, black, and green respectively.

The microcontroller board that was used with the system was an Arduino/Genuino UNO, which is an extremely simple electronics prototyping system that is designed for easily accessible prototyping (Kanda). The microcontroller that exists within the UNO's hardware is the Atmel ATmega328P chip, a low-power CMOS 8-bit microcontroller that uses an advanced

RISC architecture that has 131 instructions but executes them all on a single-clock cycle (ATMEGA328/P Datasheet).

Most of the UNO's pins were attached to an external component that performed some task. 12 of the 14 digital pins were connected to the three control signal pins on the driver, as well as additional components such as an LED and a buzzer for an alert system, a switch to switch between the program's modes, and an LCD screen for displaying messages. Four of the six analog pins were also used, two of each were connected to the two photoresistors and the two buttons for either mode of controlling the tracker's motion. Additional specifications regarding the microelectronics can be found in Appendix B.

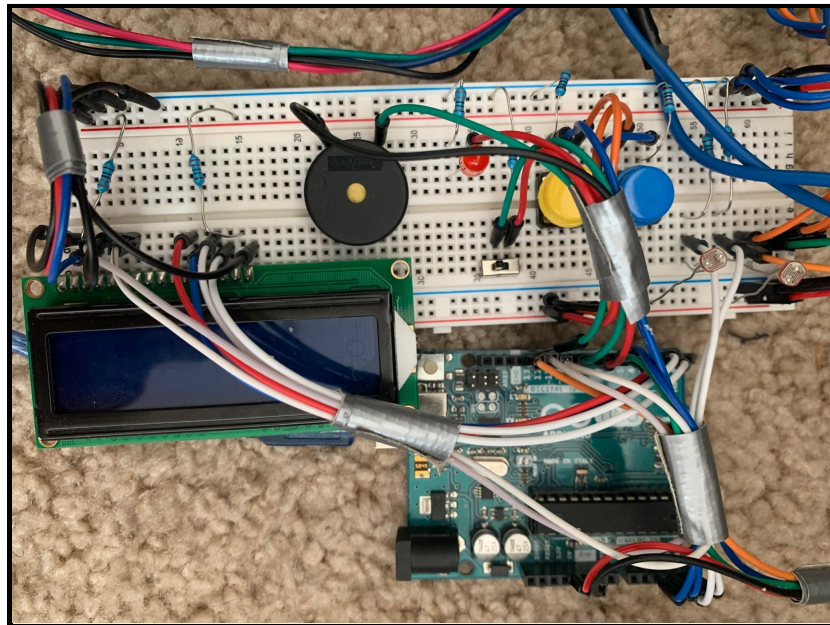


Figure 21: Close-Up Photograph of the Arduino UNO and Electronic Components.

Along with all the microelectronic components, there was a program that instructed the Arduino on what to do. The main function of the code was to receive inputs from the two photoresistors on how much sunlight was being observed by each, compare those values, and then move the motor accordingly to ensure the panel was perpendicular to the sun. Other

functions of the code were the homing function, that allowed the use of an external button to manually adjust the position of the panel, as well as the emergency function that used lights, the LED screen, and an alarm to alert the user when the panel rotates too far. Key variables included the amount of time between activating and deactivating the PUL+ terminal on the driver, which controlled the motor speed, as well as the number of steps per revolution and a counter variable that either increased or decreased depending on the direction the motor was moving. More information about both the Arduino programming software itself and the program that it helped run can be found in Appendix C.

### *5.3 Photovoltaic System*

The electrical system consists of a charge controller, inverter, and a battery to convert the DC energy from the panel to AC energy that can be used to power things, and store excess energy. This system functions as the basis for the stand-alone, battery-based solar tracking system. This system is also what provided the data for our analysis.

Our system consists of one solar module and panel. The panel is wired to a junction box with a circuit breaker on the inside. The circuit breaker is set to shut itself off automatically if it detects a current running through it of more than 16 amperes. It is also our primary means of manually disconnecting the power from the panels. The panels need to provide more voltage than the battery. 12 V nominal panels are actually ~15-17 V panels, while the panels used for this project were ~27 V panels meant for 12 or 24 V battery banks. The solar panels used were a donation from Altenergy Inc., which is now a subsidiary of Tiger Fuel Company. The panels were 280 W (STC) Solar Modules from Suniva Solar (GA), with specs shown in figure 22 below.

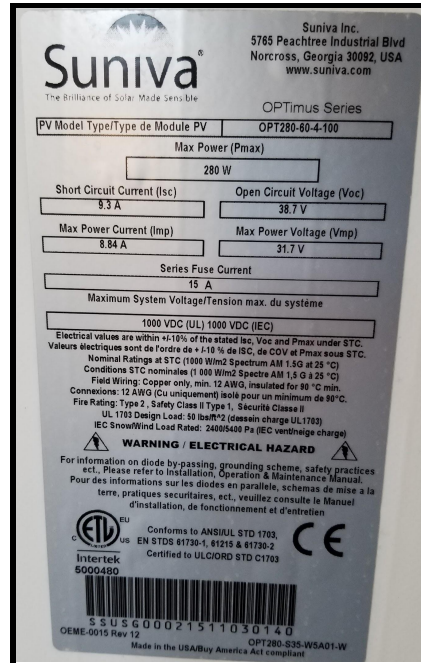


Figure 22: Specifications for the Suniva solar panels.

The circuit then runs through the charge controller, which regulates the voltage and current sent to the batteries during the charging process and then the inverter. This system used a MPPT charge controller due to its versatility with various voltages, and high efficiency. Compared to a PWM charge controller, the MPPT continually updates more quickly to get more energy out of the power from the panels. The specific model utilized in this system was the MidNite Classic 250-SL, that can handle up to 250 volts of direct current which exceeds what the 6 panels we had could create in series. The charge controller also had a small display screen that was used to manually read data, as shown in figure 23 below. There were also ethernet, usb, and RS232 ports on the charge controller that were not used, but could assist in collecting data automatically in future projects.



Figure 23: Close up of the charge controller showing the LCD screen that was used for data collection.

All main chasses (for the junction box, charge controller, and inverter) were grounded using green AWG #10 gauge wire. All the wire we used is insulated copper and stranded. Stranded wire protects against chafing and breaking under fatigue bending and is better than solid core for PV applications. The figure below was used to determine wire sizing.

CURRENT (A)	0-5	16 AWG	16 AWG	16 AWG	16 AWG	14 AWG	12 AWG	12 AWG
	5-10	16 AWG	16 AWG	14 AWG	12 AWG	10 AWG	10 AWG	10 AWG
	10-15	14 AWG	14 AWG	12 AWG	10 AWG	10 AWG	8 AWG	8 AWG
	15-20	14 AWG	12 AWG	12 AWG	10 AWG	8 AWG	6 AWG	6 AWG
	20-25	12 AWG	10 AWG	10 AWG	8 AWG	6 AWG	6 AWG	6 AWG
	25-30	10 AWG	10 AWG	10 AWG	8 AWG	6 AWG	6 AWG	4 AWG
	30-40	8 AWG	8 AWG	8 AWG	6 AWG	6 AWG	4 AWG	4 AWG
	40-50	8 AWG	8 AWG	6 AWG	6 AWG	4 AWG	4 AWG	2 AWG
	50-60	6 AWG	6 AWG	6 AWG	4 AWG	4 AWG	2 AWG	2 AWG
	60-70	6 AWG	6 AWG	4 AWG	4 AWG	2 AWG	2 AWG	1/0 AWG
	70-80	4 AWG	4 AWG	4 AWG	4 AWG	2 AWG	2 AWG	1/0 AWG
	80-90	4 AWG	4 AWG	4 AWG	2 AWG	2 AWG	1/0 AWG	1/0 AWG
	90-100	2 AWG	1/0 AWG	1/0 AWG				
	100-120	2 AWG	2 AWG	2 AWG	2 AWG	1/0 AWG	1/0 AWG	2/0 AWG
120-150	1/0 AWG	1/0 AWG	1/0 AWG	1/0 AWG	1/0 AWG	2/0 AWG	4/0 AWG	
150-200	2/0 AWG	2/0 AWG	2/0 AWG	2/0 AWG	2/0 AWG	4/0 AWG	4/0 AWG	
	0-4	4-7	7-10	10-15	15-20	20-25	25-30	
	LENGTH IN FEET							

Figure 24: Chart detailing the current capacity for different lengths and types of wires. (*Dragonfly Energy, 2021*)

Any further modifications would need to adjust wire gauges, since the current set up is designed for use with a singular panel only.

The most dangerous component in the system is the inverter, so a Renogy brand inverter was chosen with built-in ground fault protection and outlets. For small systems, a stand-alone central inverter is best. Micro-inverters are best suited for large arrays experiencing varying shading effects across the array. Systems connected to the grid need grid-suited inverters, but since this project was always intended to be off grid, the stand alone inverter proved to be the best option.

The battery was a battle born battery that was programmed specifically for the charge controller according to the instructions detailed in Appendix D. The battery is lead-acid which releases flammable hydrogen gas, so it needs to be kept in a well ventilated area. Battle born batteries warrant 4 batteries in series, and additional battery storage could be added for simultaneous testing of panels.

The full set up was arranged on a painted piece of wood for ease of access and transportability, shown in figure 25 below.



Figure 25: The full PV set up on the mounting board.

## **6. Methodology**

To reduce costs, it was not feasible to safely test multiple modules at once according to the safety ratings of our PV equipment. To combat this, multiple testing periods took place from 11 AM - 3 PM with one rig (either control or tracking) being tested for the first two hours, and then switching to the other rig at solar noon, around 1:00 pm, when the sun is directly above the testing location, and testing it for the next two hours. Multiple days of testing were averaged to reduce error, and the first rig to be tested was switched as well.

The data was collected manually at 10 min intervals, recording the voltage and current readings from the charge controller. This resulted in four data points; voltage from the PV panel, wattage from the PV panel, voltage in the battery, and current in the battery. Since clouds have a significant scattering effect, data was collected on clear days and at times when clouds were not clearly obstructing the sun, to ensure more consistent data. Additionally, the battery needed to be drained before every testing period since the data would be inaccurate if it were full.

Three different setups were tested, a flat stationary panel, an angled stationary panel, and the angled tracking panel. The same solar panel was used for all of the testing to reduce any error in panel efficiency. Day 1 of testing occurred on 4/16/2022 and consisted of comparing the flat panel to the tracking panel, and day 2 of testing occurred on 4/23/2022 and consisted of comparing the angled stationary panel to the tracking panel.

## **7. Results**

The results from the two days of testing are plotted in figures 26 and 27 below. The blue line represents the tracking panel, and the orange line represents the stationary panel for the day.

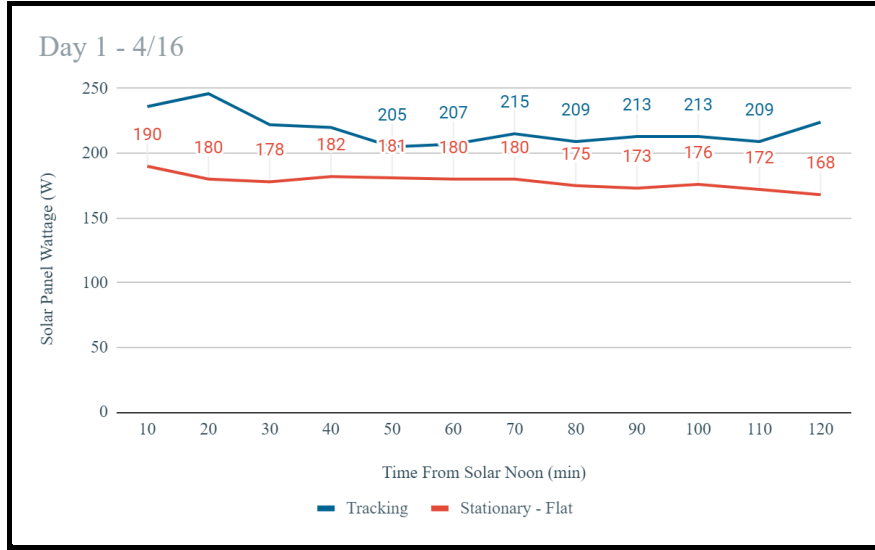


Figure 26: Testing results of the tracking panel (blue line) vs the stationary, flat, panel (orange line) from 4/16.

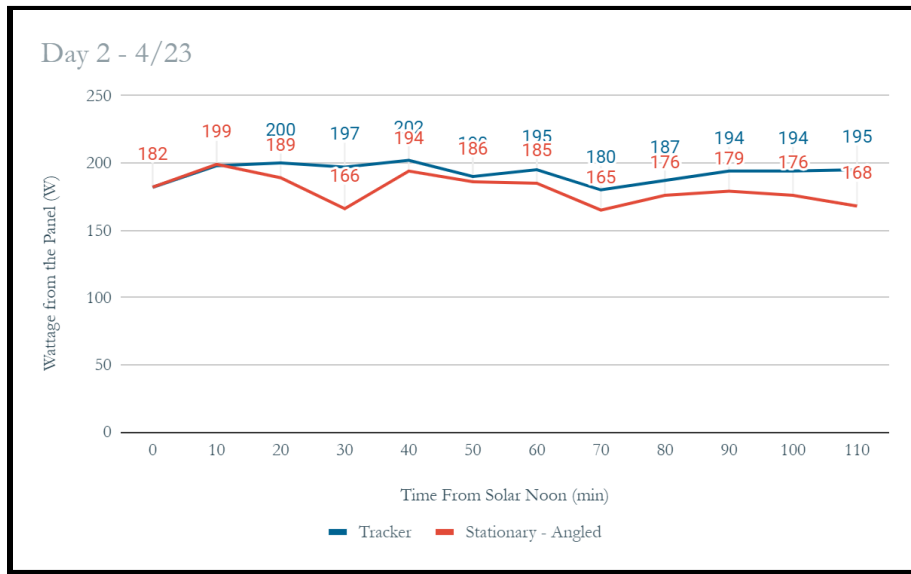


Figure 27: Testing results of the tracking panel (blue line) vs the stationary, angled, panel (orange line) from 4/23.

The results are also summarized in table I, below.

Table I: Summarized data from both days of testing the various solar panel setups.

Testing Day	Panel Type	Average Panel Voltage	Average Panel Wattage	Average Battery Voltage	Average Battery Amperage
1 (4/16)	Flat stationary	26.4	178	12.6	14.2
1 (4/16)	Tracking	27.1	218	13	16.9
2 (4/23)	Flat Tilted	25.4	180	13.3	13.5
2 (4/23)	Tracking	25.6	193	13.4	14.1

These results indicated an 18.5% improvement for efficiency on day one of the tracking panel when compared to a flat panel, and a 6.4% increased efficiency on day two when compared to the angled stationary panel.

On the qualitative side, both testing days were observed to be sunny and clear, with minimal cloud coverage. Other weather factors are summarized below in table II.

Table II: Various weather details for both days of testing.

Date	UV Index	Wind (MPH)	Temperature (F)
4/16	8	29	81
4/23	7	17	84

### 7.1 Challenges

Since the data was recorded manually, if a cloud was passing by the sun during collection time, the team waited until it passed to get more accurate readings. Clouds scatter sunlight and decrease the efficiency of all panel setups significantly, lowering the wattage from the panels. Testing was only able to occur on clear days which constrained the amount of data collected, and there was no precise way of quantifying any cloud coverage that occurred. In the figure below

the analog readings of the photoresistors are graphed, regions where there are large dips in the readings are time spans where cloud coverage was blocking the sun. In the mostly sunny days that were tested this could bring the panels wattage down the 20-70% of its potential output

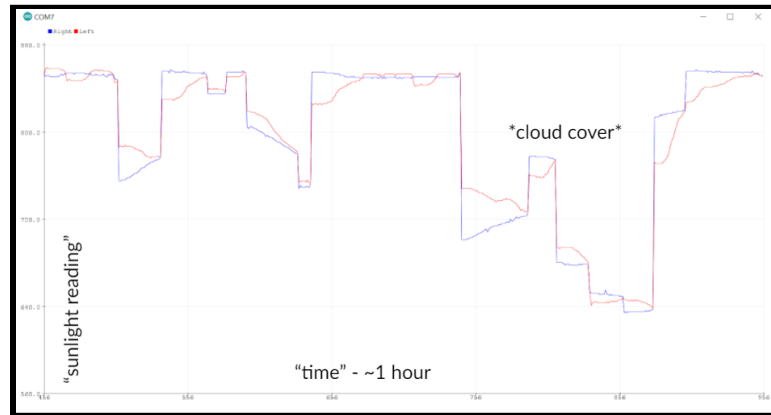


Figure 28: Showing the analog reading of the left and right photoresistors during an hour of testing.

One way to remove environmental factors such as weather conditions would be to test multiple systems simultaneously. Since our PV equipment was not rated to handle the current that would occur from multiple panels, only one system at a time could be tested. In the future, simultaneous testing would allow for more conclusive data.

Vibrations due to wind were a concern. On days of high wind (day 1 of testing), the panel and shaft would oscillate. The amplitude of this oscillation was observed to be as much as 5 degrees. Large vibration is a structural concern. A high amount of vibrations can lead to extra stress due to fluctuating loads.

Another factor that constrained our data was a limited testing time. Due to limited availability within the group as well as the need to carefully monitor the system the entire time it ran resulted in testing windows of 4 hours. As shown in figure 8, the largest increase of efficiency with a tracking panel occurs closer to sunrise and sunset. This is due to the stationary panel being in optimal position around solar noon, which causes there to be minimal difference between the tracking panel around that time.

## 7.2 Comparison to Projected Data

The projected data calculated previously and summarized in figure 8, was also compared. Since the testing period was limited to a few hours in the day, figure 29 below shows the relevant section of figure 8. As mentioned earlier the irradiance calculations were done by making a fair amount of assumptions, this includes: solar panel efficiency, atmospheric scattering, and was also calculated for a day in november.

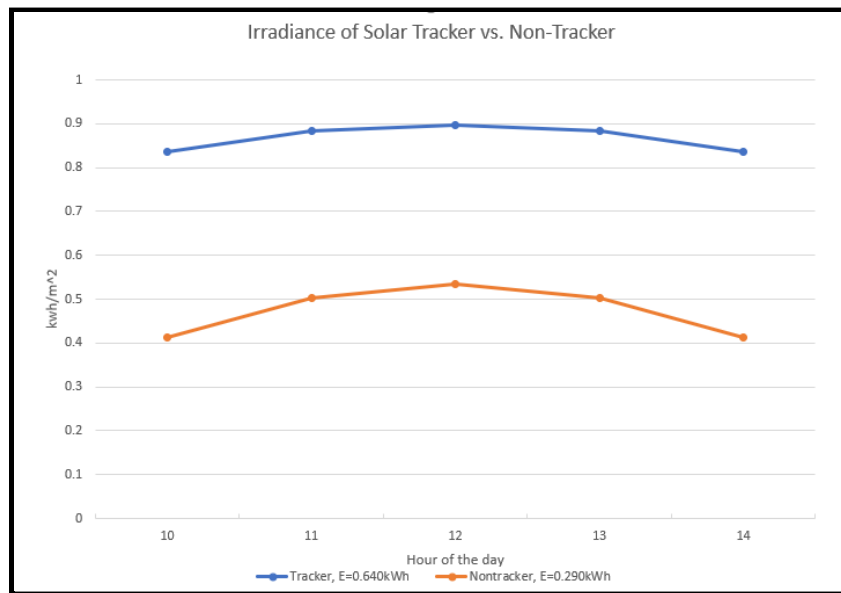


Figure 29: Projected irradiance of a solar tracker and stationary, flat, panel from 10am-12pm.

Figure 30 below, shows the results from the tracking system with second order polynomial fit lines. Looking between both graphs it is notable that the irradiance in from the data is much lower overall than the irradiance from the calculations, this is mostly due to the assumption that the solar panels were running at high efficiency and that there is very little light being scattered by the atmosphere. The difference between the tracking and non-tracking are mainly from the difference in time of year; projected irradiation was for the month of november while testing was done in april. This would give the non-tracker more kWh of energy because the sun orientation in the sky would be higher.

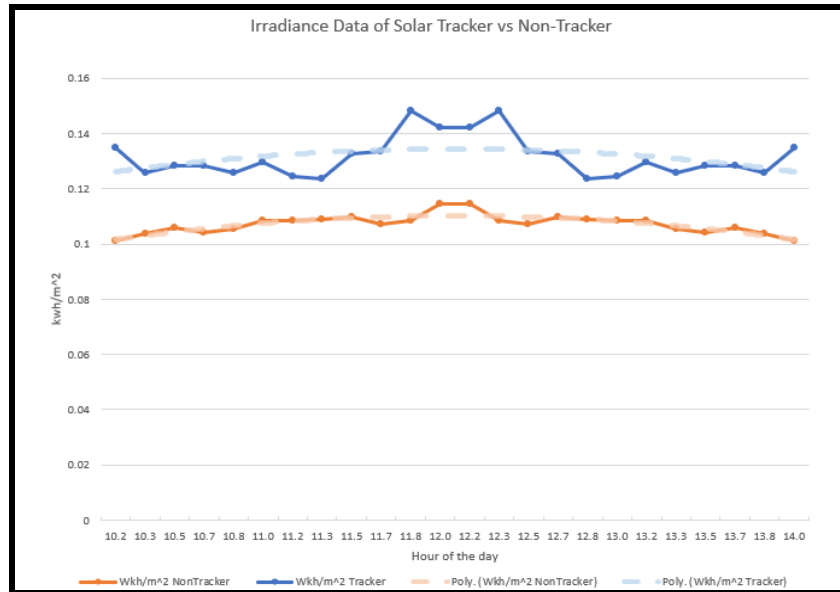


Figure 30: Testing results of the tracking panel (blue line) vs the stationary, flat, panel (orange line) from 4/16.

## 8. Analysis

Overall, the first round of full-scale testing was successful. While various design constraints limited this project from reaching statistically conclusive data, the results indicate a clear positive sign that the tracker is working as projected. The tracking devices outperformed the stationary panels on both days, and figure 27, shows an increased divergence in the panel efficiency at the end of the testing period. This divergence is a positive sign that if testing were to continue closer to sunrise and sunset, the efficiency of the tracking panel would be even more significant.

When comparing the data collected by the panel to the data predicted in figure 8, there are some key differences. First, the y-axis on the plot, kWh, are significantly different in the real case, which is likely due to the efficiency limitations of the panel itself and the assumptions of a 'perfect system' when making the projection. The fit lines show that the shape of the plot was

predicted well, but expansion of testing later or earlier into the day could provide more conclusive evidence on the shape of the curves.

### *8.1 Cost analysis*

According to the EIA (2021), the average American household uses approximately 10,715 kWh of electricity per year. With the cost of electricity in Virginia being around 11.66 cents per kWh, that is around \$1250 spent per year on electricity (Dominion Energy, 2020). With the increased efficiency of 18.5% that occurred on testing day 1, that would result in savings equivalent to approximately \$231 per year and with the efficiency increase of 6.4%, the savings would be approximately \$80 per year. While the cost of creating a single tracking system is significantly larger than a commercialized product would be, the monetary savings are likely not significant enough to motivate household owners to pursue tracking devices.

## **9. Future Work**

This project was intended to continue on in future years, and there are many directions this work can be expanded on. The most important expansion of this work would be to perform additional testing and certify any results. Replicating the testing done here would be beneficial, but expanding the testing window to capture the entire day would likely lead to additional conclusions.

Adjusting the PV system to allow for better testing is another significant area for improvement. First, the capacity of the battery and wiring could be adjusted to allow for the testing of multiple panels at the same time. Up to 4 of the battle born batteries can be wired up in series, allowing for a significantly larger capacity for running multiple panels. The inverter is also only rated for 12 VDC so would need to be upgraded as well. This would take away any

factors such as weather when conducting tests to compare systems, and could allow for more passive testing. Additionally, the PV components could be arranged and secured in a weather proof manner, so testing could occur in all weather. Currently, some components are suited to sit in the sun for extended periods, and many of the components are not waterproof. Typically these types of components are stored in a ventilated and covered area, and doing so for this project would also help ensure that long periods of testing were possible.

Another key function of this project was applying the system to the reCOVER house at Milton Airfield. The rig was designed for rooftop installation, but additional steps are needed before it is ready to be installed. Ensuring the structural integrity of the roof itself is the first step, and making sure that multiple rigs could safely be mounted is essential. Another factor to consider is the effect of wind force. Simulations on the rig design can help predict the effect of wind gusts and provide information on how to adjust our design if necessary. Development of reliable wind data is underway by NREL and others but still in early stages, so it was hard to get the facts on this new field of inquiry (Yingchen).

Wind and the resulting vibrations are another area that future designs could address. An extra bearing on the shaft would likely supply enough support to reduce these effects, but there are other potential solutions. The shaft could also be replaced with a hollow tube, or hydraulic dampeners could be added to the system. Additionally, the entire rotary design could be reimagined and linear actuators could provide the turning force for the panel. Actuators could be installed on the side of the panel and provide the force to bring the side up or down. This could likely be accomplished with one actuator, but up to four could be used for a dual axis system.

Lastly, the energy generation set up can hopefully be one day connected to the ground-source heat pump to sustainably manage the HVAC of the reCOVER House. As

previously stated, the energy needs of the pump are unknown since a scale design has not yet been created, but the two teams would need to work in conjunction to ensure a reliable energy supply from the panels.

## **10. Conclusion**

A single-axis closed-loop fully functional solar tracking panel was successfully created. A thorough literature review helped evaluate existing designs and potential areas for innovation, and an extensive prototyping phase narrowed down the designs to then create a full scale model. A custom rig was designed, modeled, and built, incorporating technical requirements with aesthetic factors, to one day be installed on top of a roof. A NEMA-23 stepper motor was used in conjunction with photoresistors and various microelectronic parts to create the tracking component of the system, which fed into the worm gear that turned the panel. The tracking system was equipped with homing and tracking modes, as well as with features such as the alert system to ensure the solar panel does not rotate into the ground. Lastly, a PV system was installed to convert the solar energy to usable electricity, and provide the tools for data collection.

Two testing days occurred to compare the tracking system to a flat and angled stationary panel. The results indicated that the tracking panels did increase the efficiency of energy generation, though additional testing is needed to make conclusive results. There are numerous ways to expand this project into the future, and further develop the knowledge base of solar tracking panels.

## 11. References

- “NEMA 17 Bipolar 45NCM (64OZ.In) 2A 42x42x40mm 4 Wires W/ 1M Cable & Connector.” *STEPPERONLINE*, 4 Nov. 2020, <https://www.omc-stepperonline.com/nema-17-bipolar-45ncm-64oz-in-2a-42x42x40mm-4-wires-w-1m-cable-connector-17hs16-2004s1>
- “24V NEMA 23 Stepper Motor ok57sth56-2804A.” *Scion Electronics*, 4 Feb. 2021, <https://scionelectronics.com/product/24v-nema-23-stepper-motor-ok57sth56-2804a/>
- “Affordable Electric Rates: Virginia.” *Dominion Energy*, 1 Nov. 2020, <https://www.dominionenergy.com/virginia/rates-and-tariffs/affordable-rates#:~:text=Base%20on%20rates%20in%20effect,rate%20of%20about%2011.66%20cents>
- “Arduino UNO & Genuino UNO.” *Arduino*, 1 May, 2021, <https://www.arduino.cc/en/main/arduinoBoardUno>
- ATMEGA328/P Datasheet Summary*. Atmel, 2016, <https://datasheet.octopart.com/ATMEGA328P-MU-Microchip-datasheet-65729177.pdf>
- Chowdhury, Muhammad EH, et al. "A low-cost closed-loop solar tracking system based on the sun position algorithm." *Journal of Sensors* (2019). <https://doi.org/10.1155/2019/3681031>
- Clifford, M. J., and D. Eastwood. "Design of a novel passive solar tracker." *Solar Energy* 77.3 (2004): 269-280. <https://doi.org/10.1016/j.solener.2004.06.009>
- DM542T(v4.0) Full Datasheet Digital Stepper Driver*. StepperOnline, Oct. 2020, [https://www.omc-stepperonline.com/download/DM542T\\_V4.0.pdf](https://www.omc-stepperonline.com/download/DM542T_V4.0.pdf)
- Model BB10012|BB10012H 100Ah 12V Deep Cycle LiFePO4 Battery Manual and Installation Guide*. Dragonfly Energy, 2021, <https://t1t1pye1e13di20waq11old70-wpengine.netdna-ssl.com/wp-content/uploads/2021/02/BB10012-BB10012H-Manual.pdf>.
- “Frequently Asked Questions (Faqs) - .” *EIA*, U.S. Energy Information Administration (EIA), 7 Oct. 2021, <https://www.eia.gov/tools/faqs/faq.php?id=97&t=3#:~:text=How%20much%20electricity%20does%20an,about%20893%20kWh%20per%20month>
- “History of Solar Energy: Who Invented Solar Panels?” *Vivint.Solar*, Retrieved May 5, 2022, <https://www.vivintsolar.com/learning-center/history-of-solar-energy>
- Honsberg, C., & Bowden, S. (n.d.). *Terrestrial Solar Radiation*. PVEducation. Retrieved December 13, 2021, from <https://www.pveducation.org/pvcdrom/acknowledgements>
- Jørgensen, S.E. “Exergy.” *Encyclopedia of Ecology*, 2008, pp. 1498–1509., <https://doi.org/10.1016/b978-008045405-4.00689-3>

- Lowe, Doug. "Alternating Current in Electronics: Hot, Neutral, and Ground Wires." *Electronics All-in-One for Dummies*, 3rd ed., John Wiley & Sons, Inc., Hoboken, NJ, 2022, <https://www.dummies.com/article/technology/electronics/circuitry/alternating-current-in-electronics-hot-neutral-and-ground-wires-179852/>. Accessed 6 May 2022.
- Moran, Michael J., et al. *Fundamentals of Engineering Thermodynamics*. John Wiley & Sons, Inc., 2018.
- Mpodi, Emmanuel Karabo, Zeundjua Tjiparuro, and Oduetse Matsebe. "Review of dual axis solar tracking and development of its functional model." *Procedia Manufacturing* 35 (2019): 580-588. <https://doi.org/10.1016/j.promfg.2019.05.082>
- "PDF 28BYJ-48 Data Sheet ( Hoja De Datos )." DataSheet, 2020, <http://www.datasheet.es/PDF/1006817/28BYJ-48-pdf.html>.
- Regalbuto, C. (2014, March 21). *The Exergy of Nuclear Fuels and Nuclear Radiation*. The exergy of nuclear fuels and nuclear radiation. Retrieved November 22, 2021, from <http://large.stanford.edu/courses/2014/ph241/regalbuto1/>
- Saltelli, Andrea. "Sensitivity Analysis for Importance Assessment." *Risk Analysis*, vol. 22, no. 3, 2002, pp. 579–590., <https://doi.org/10.1111/0272-4332.00040>.
- Seme, Sebastijan, et al. "Solar photovoltaic tracking systems for electricity generation: A review." *Energies* 13.16 (2020): 4224.<https://doi.org/10.3390/en13164224>
- Teja, Ravi. "Arduino Uno Pinout, Specifications, Board Layout, Pin Description." *Electronics Hub*, 18 Sept. 2021, <https://www.electronicshub.org/arduino-uno-pinout/>
- "The History of Solar - Energy." *Energy Efficiency and Renewable Energy*, US Department of Energy, 2002, [https://www1.eere.energy.gov/solar/pdfs/solar\\_timeline.pdf](https://www1.eere.energy.gov/solar/pdfs/solar_timeline.pdf)
- Unbound Solar. (2015). *Suniva Optimus Series Monocrystalline Solar Modules*. <https://documents.unboundsolar.com/media/suniva-opt285-60-4-100-silver-mono-solar-panel-specs-2917622048-4.pdf>
- Veligorskyi, O., Kosenko, R., & Stepenko, S. (2014, June). High-efficiency solar tracker development and effectiveness estimation. In *2014 IEEE International Conference on Intelligent Energy and Power Systems (IEPS)* (pp. 153-158). IEEE. <https://doi-org.proxy01.its.virginia.edu/10.1109/IEPS.2014.6874169>
- Vis, Peter J. *Led Resistor Calculator*, Retrieved May 2, 2022, <https://www.petervis.com/electronics/led/led-resistor-calculator.html>
- "What Is Arduino and Arduino Alternatives." *What Is Arduino? | Arduino Alternative*, Kanda, Retrieved May 2, 2022, <https://www.kanda.com/what-is-arduino.php>

Yingchen, Zhang. "Solar and Wind Forecasting." *Solar and Wind Forecasting*, NREL Transforming Energy, Retrieved May 3, 2022,  
<https://www.nrel.gov/grid/solar-wind-forecasting.html>

## Appendix A: Microstep Driver Additional Specifications

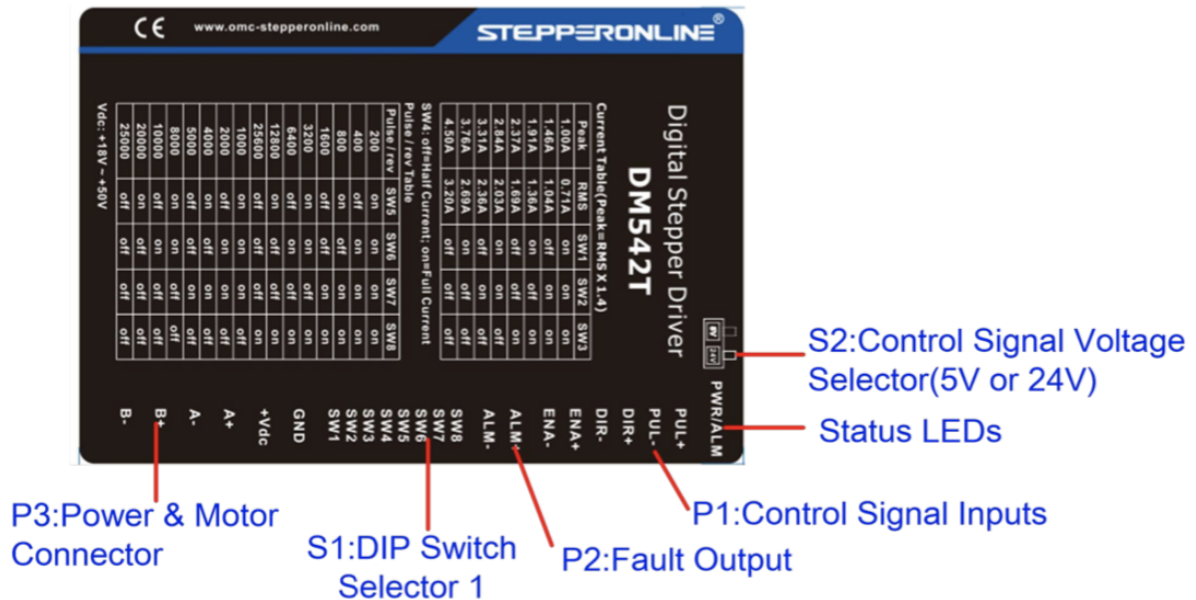


Figure A1: Systematically Labeled Diagram of the Microstep Driver (*DM542T(v4.0) full Datasheet Digital Stepper driver 1.0-4.2a 20-50VDC ...*)

The driver's output pins are arranged in three connector blocks that all serve distinct purposes. The first, referred to in the user manual as P1, allows for the reception of control signals from the microcontroller and thus, allows for the driver's control of the motor's movements. The pins that make up P1 are abbreviated as such: PUL+ and PUL- each control one individual step, DIR+ and DIR- control the motor's direction, and ENA+ and ENA- can temporarily and spontaneously disable the drive by 4.5-24V and enable the drive by 0-0.05V. PUL+, DIR+, and ENA+ are the positive terminal pins for each function that are connected to three corresponding digital I/O pins of the microcontroller, while PUL-, DIR-, and ENA- are simply the negative terminals for each function that are directly hooked up to ground in a common cathode connection, even though this layout can also support common anode connections if the microcontroller uses an open-collector signal. Each of these pins are optically

isolated, meaning that they are powered on and off by optically transferred signals using an optocoupler.

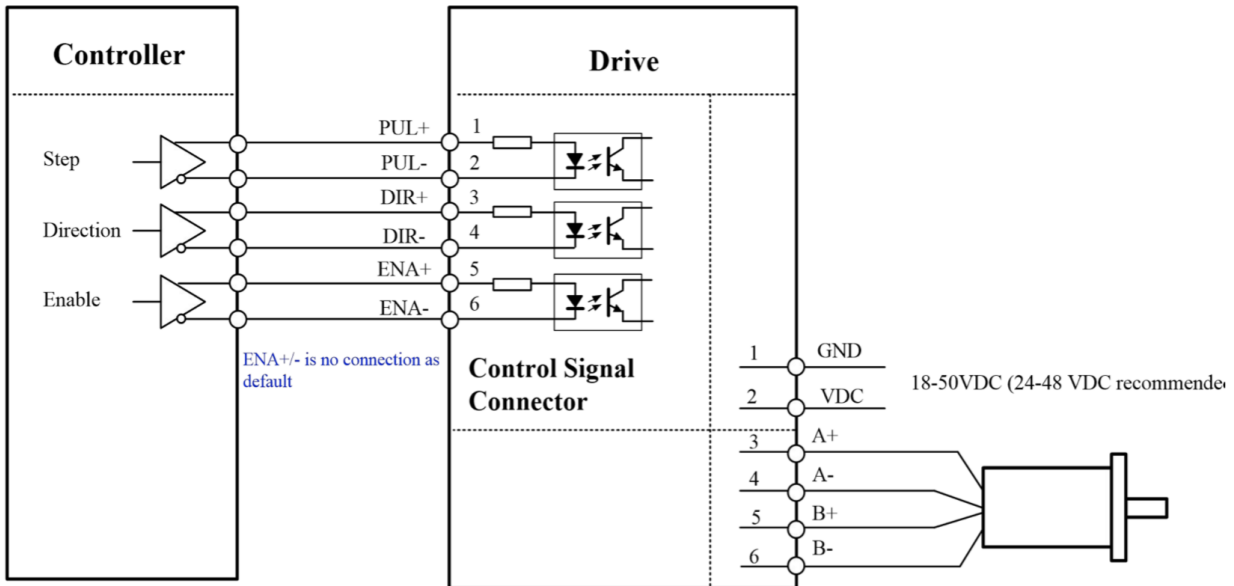


Figure A2: Simplified Schematic of the Driver Connected to a Controller and a Motor (*DM542T(v4.0) full Datasheet Digital Stepper driver 1.0-4.2a 20-50VDC ...*)

PIN	Details
<b>PUL+</b>	Pulse and Direction Connection: <b>(1)</b> Optically isolated, high level 4.5-5V or 24V, low voltage 0-0.5V <b>(2)</b> Maximum 200 KHz input frequency <b>(3)</b> The width of PUL signal is at least 2.5 $\mu$ s, duty cycle is recommended 50% <b>(4)</b> DIR signal requires advance PUL signal minimum 5 $\mu$ s in single pulse mode <b>(5)</b> The factory setting of control signal voltage is 24V, <b>must need</b> to set S2 (figure 2) if it is 5V
<b>PUL-</b>	
<b>DIR+</b>	
<b>DIR-</b>	
<b>ENA+</b>	
<b>ENA-</b>	<b>(3)</b> ENA signal requires advance DIR signal minimum 5 $\mu$ s in single pulse mode <b>(4)</b> Enable time to be at least 200ms

Figure A3: Tabulated Specifications for the P1 Connector Block on the DM542T (*DM542T(v4.0) full Datasheet Digital Stepper driver 1.0-4.2a 20-50VDC ...*)

The second connector block, P2, serves as fault protection for the stepper driver and consists of the pins ALM+ and ALM-. These two pins can be connected in series with a 5-24V

battery, such as the aforementioned power supply, and a load (preferably a resistor in either sinking or sourcing, which means that the load can be connected either between ALM+ and the positive terminal (sourcing) or ALM- and the negative terminal (sinking). Although fault protection is optional, when these two pins are connected in this way, the red LED on the right side of the driver will flash whenever peak current exceeds the limit (over-current protection) or if the drive working voltage exceeds 60V (over-voltage protection). In either case, the sequence of flashes will be different from one another depending on the scenario.

Pin	Details
ALM+	(1) Maximum 30V/100mA output (2) Sinking or sourcing
ALM-	(3) The resistance between ALM+ and ALM- is low impedance as default, and will change to high when the drive goes into error protection. (4) Fault connection refer to <a href="#">chapter 4.2</a>

Figure A4: Tabulated Specifications for the P2 Connector Block on the DM542T (*DM542T(v4.0) full Datasheet Digital Stepper driver 1.0-4.2a 20-50VDC ...*)

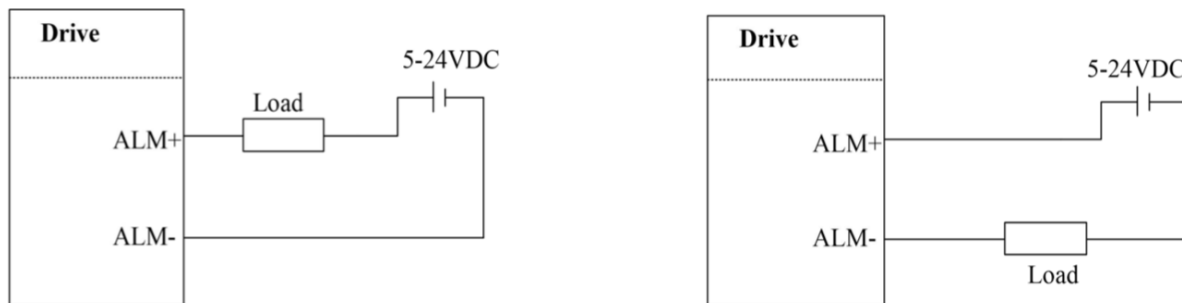


Figure A5: Sourcing and Sinking Configurations for ALM +/- Pins Connected in Series with Load and Battery (*DM542T(v4.0) full Datasheet Digital Stepper driver 1.0-4.2a 20-50VDC ...*)

The third controller block, P3, functions as a motor and power supply connector, with the pins A+ and A- functioning as direct connections to motor phase A and B+ and B- as connections to motor phase B. The pins Vdc and GND connect to the positive and negative terminals of the power supply. Although the driver can power a range of stepper sizes, supply voltage and output current magnitudes must be taken into consideration. Higher supply voltages

allow for higher motor speeds to be achieved while output current determines the motor's torque. For this system, stepper speed is not a factor that determines performance, and so because of the higher risk of noise, vibration, and heating with a higher supply voltage, it was determined that it would be best to minimize this quantity.

Pin Function	Details
GND	Power supply ground connection.
+Vdc	Power supply positive connection. Suggest 24-48VDC power supply voltage
A+, A-	Motor Phase A connections. Connect motor A+ wire to A+ Pin; motor A- wire to A-
B+, B-	Motor Phase B connections. Connect motor B+ wire to B+ Pin; motor B- wire to B-

Figure A6: Tabulated Specifications for the P3 Connector Block on the DM542T (*DM542T(v4.0) full Datasheet Digital Stepper driver 1.0-4.2a 20-50VDC ...*)

The stepper has an 8-bit DIP switch, which is used for the dual purpose of current configuration and microstep resolution. The first three switches from the left, labeled SW1-3, control the output current. As mentioned previously, the minimum peak current is 1.0A and the maximum peak current is 4.5A. This quantity can be manually varied through the use of these switches and different current levels can be obtained by the different permutations in which these switches are turned on and off. As a general rule with a few exceptions, more switches turned on means a lower peak current. If all switches are switched on, the peak current is at 1.0A while turning off all switches maximizes the peak current to 4.5A. The four switches from the right, labeled SW5-7, control the microstep resolution and work the same way as the three switches that control peak current. If more are turned on, the lower the microstep resolution. The number of steps per revolution ranges from 200 (full-step mode) to 25000 (1/125 microstep).

Peak Current	RMS Current	SW1	SW2	SW3
1.00A	0.71A	ON	ON	ON
1.46A	1.04A	OFF	ON	ON
1.91A	1.36A	ON	OFF	ON
2.37A	1.69A	OFF	OFF	ON
2.84A	2.03A	ON	ON	OFF
3.31A	2.36A	OFF	ON	OFF
3.76A	2.69A	ON	OFF	OFF
4.50A	3.20A	OFF	OFF	OFF

Figure A7: The Effects of the States of Switches 1-3 on the Peak and RMS Current Powering the Motor  
(*DM542T(v4.0) full Datasheet Digital Stepper driver 1.0-4.2a 20-50VDC ...*)

Microstep	Steps/rev.(for 1.8°motor)	SW5	SW6	SW7	SW8
1	200	ON	ON	ON	ON
2	400	OFF	ON	ON	ON
4	800	ON	OFF	ON	ON
8	1600	OFF	OFF	ON	ON
16	3200	ON	ON	OFF	ON
32	6400	OFF	ON	OFF	ON
64	12800	ON	OFF	OFF	ON
128	25600	OFF	OFF	OFF	ON
5	1000	ON	ON	ON	OFF
10	2000	OFF	ON	ON	OFF
20	4000	ON	OFF	ON	OFF
25	5000	OFF	OFF	ON	OFF
40	8000	ON	ON	OFF	OFF
50	10000	OFF	ON	OFF	OFF
100	20000	ON	OFF	OFF	OFF
125	25000	OFF	OFF	OFF	OFF

Figure A8: The Effects of the States of Switches 5-7 on the Motor's Microstep Resolution (*DM542T(v4.0) full Datasheet Digital Stepper driver 1.0-4.2a 20-50VDC ...*)

## Appendix B: Arduino UNO and ATmega328P - Additional Specifications

The ATmega328P has 32 KB of flash memory, with 0.5 KB of which occupied by the bootloader, that allows the user to upload new code to it without the use of an external hardware programmer. In addition, the ATmega328P has 2 KB of SRAM and 1 KB of EEPROM. In addition, the UNO, as well as other Arduino boards such as the Nano and Mega 2560, use an open-source integrated development environment (IDE) which is used for programming the microcontroller, which is done in C++ with the addition of several extra functions.

The UNO is externally powered by either a USB port or either an AC or DC external power supply, whose leads can be inserted into the Vin and GND pin headers of the power connector. In addition, the power supply can be connected to a power jack, allowing for the Vin pin to be used as an output rather than an input. The range of input voltages from an external source is 6-20V. However, the recommended voltage range for an external power source is 7-12V, since anything below 7V might cause the 5V pin to supply less than 5V and cause the board to become unstable and anything above 12V will overheat the voltage regulator. There are multiple power pins on the UNO, including a Vin pin, regulated 5V and 3.3V output pins, ground pins, and a voltage reference pin.

There are 14 digital I/O pins, labeled 0-13. These pins can perform digital-analog conversion operations with functions like `digitalRead()` and `digitalWrite()`, as well as I/O assignments with the function `pinMode()`. Similarly, the 6 analog pins, labeled A0-A5, use functions like `analogRead()` and `analogWrite()` to perform analog-digital conversion. Most of the board's digital I/O pins have various specialized functions, such as 8-bit PWM output, SPI communication, serial data transmission using pins 0 and 1 to receive (RX)

and transmit (TX) data respectively, and external interrupts using the `attachInterrupt()` function (*Arduino UNO & Genuino UNO*).

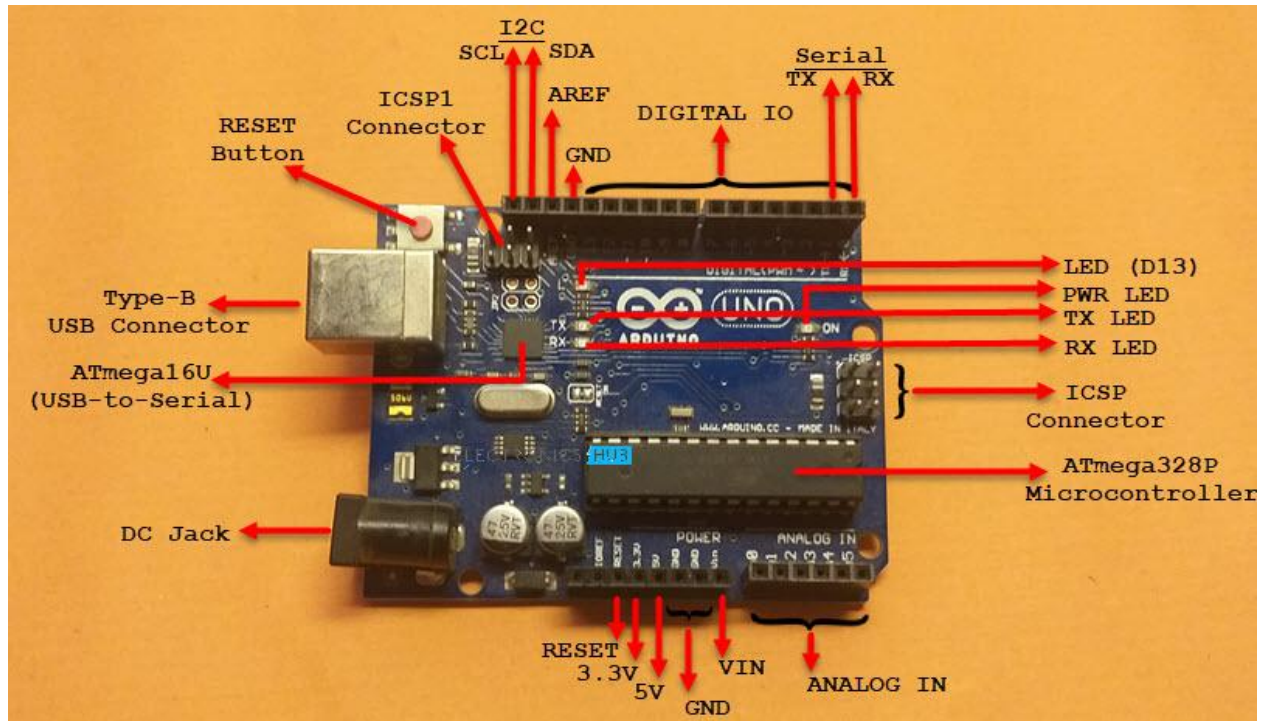


Figure B1: Systematically Labeled Photograph of the Arduino UNO, taken from <https://www.electronicshub.org/arduino-uno-pinout/> (Teja)

The PUL+, DIR+, and ENA+ pins on the driver were attached to various digital pins on the UNO. In addition, other components such as an LED, a piezo buzzer, and a toggle switch were attached to other digital pins due to their operation being based on either an on/off state or an internal command, as was the case with the buzzer, which used the `tone()` and `noTone()` functions. The remainder of the digital pins were used to power an LCM1602C liquid crystal display screen, whose function was to display visual messages, including the mode that the system was in and emergency messages. The analog pins were used as inputs for photoresistor and push button data, which were responsible for both the automatic and manual control of the

motor, respectively. Because the motor could only turn in either a clockwise or counterclockwise direction, there were two photoresistors and two buttons, meaning that four of the six analog inputs were used. Some components, such as the LED, were connected to ground with a pull-down resistor to prevent short-circuiting. However, other components, such as the buzzer, do not require any resistors in series in order to function properly. The only parts of the circuit design where resistance values needed to be taken into account are with the photoresistors, where the resistors attached to them must have equal resistance values to balance the voltage drop between them, and the LED, with a forward voltage range of 1.8-2.2V and a forward current rating of 20-30mA (Vin).

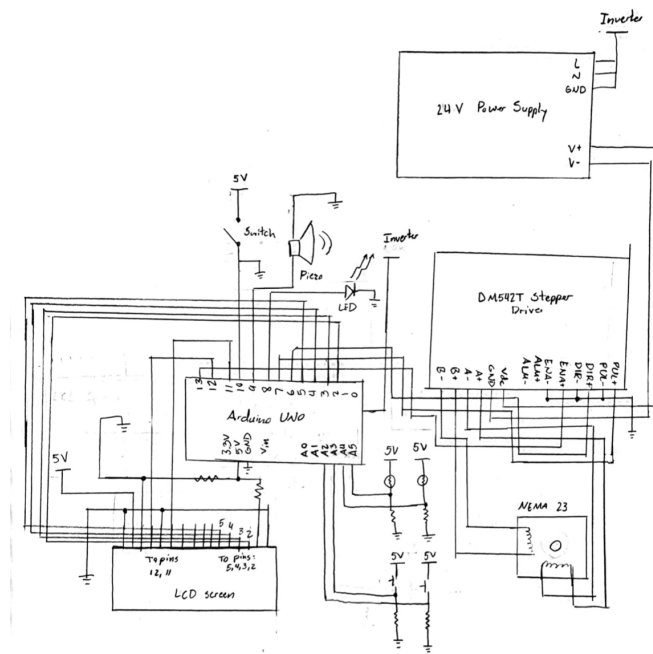


Figure B2: Full Hand-Drawn Schematic of the Microelectronic System

## Appendix C: Arduino IDE Features and Programming

The design's programming consists of a section that assigns each variable to a pin for later use within the code, a method for initializing each variable for completing each task (setup function), a method providing a continuous loop for the program to run during operation (loop function), and three smaller functions that are called on throughout this loop that perform smaller tasks such as moving the stepper motor by a specified number of steps in either direction, displaying variables on the Arduino IDE's serial monitor, and initiating an emergency message in case the motor continuously moves in one direction. The LiquidCrystal library is imported into the code using `#include`. Some variables that get called upon during operation are one that specifies the delay in microseconds between the switching on and off of the driver's step pin, the difference between the analog photoresistor readings converted to digital values, and a counter that increases or decreases as the motor moves in a particular direction and triggers the aforementioned emergency message. There are two primary modes that the system can operate in depending on the on/off state of the switch: homing mode, which uses the manual input of the pushbuttons to control the motor, and tracking mode, which uses photoresistor readings to perform the same task. Photoresistor readings can be seen in both numerical and graphical format in real time with the serial monitor and plotter, respectively. These tools are also built into the Arduino IDE and are highly useful for observing how these quantities change as the motor orients itself towards the sun, as well as what happens during periods of cloud coverage.

```
// Libraries to add
#include <LiquidCrystal.h>

// LCD digital pins
LiquidCrystal lcd(12, 11, 5, 4, 3, 2);

// Digital pins:
const int dirPin = 6;
```

```

const int stepPin = 7;
const int led = 8;
const int buzzer = 9;
const int toggle = 10;
const int enable = 13;

// Analog pins:
const int leftButton = A2;
const int rightButton = A3;
const int leftSensor = A4;
const int rightSensor = A5;

// Constants
const int stepper_speed = 8000;
const int stepsPerRevolution = 200;
const int bit_difference = 5; // This value goes up to 1024
// When you lower the resistance of the resistors, you have to lower this value.
// This is because there is less of a voltage drop across each resistor, and since
// pins A0 and A1 read the voltage drop across the resistor, the digital equivalents
// of these analog-read values compute to a lower number of bits.

// Variables
int digitalValue_left = 0;
int digitalValue_right = 0;
int counter = 0;

void setup() {

  Serial.begin(9600);

  // initialize analog pins (buttons & photoresistors) as inputs
  pinMode(leftSensor, INPUT);
  pinMode(rightSensor, INPUT);
  pinMode(leftButton, INPUT);
  pinMode(rightButton, INPUT);

  // initialize switch as input
  pinMode(toggle, INPUT);

  // initialize digital pins as outputs
  pinMode(led, OUTPUT);
  pinMode(buzzer, OUTPUT);
  noTone(analogRead(buzzer));
  pinMode(stepPin, OUTPUT);
  pinMode(dirPin, OUTPUT);
  pinMode(enable, OUTPUT);

  // initialize LCD screen
  lcd.begin(16, 2);
}

void loop() {

  //////////////////////////////////// TRACKING MODE ////////////////////////////////////

  if (digitalRead(toggle) == HIGH) {

    // performs analog-digital conversion on the left and right sensor pins (A4 and A5)
    digitalValue_left = analogRead(leftSensor);
    digitalValue_right = analogRead(rightSensor);
  }
}

```

```

// Checks to see if panel is tilted too far to one side
if (abs(counter) > stepsPerRevolution / 2) {
  // If it is, set the enable pin to HIGH to stop the stepper motor while it's moving and
  // set off the alarm
  digitalWrite(enable, HIGH);
  emergency_message();
} else {
  // If not, initiate tracking mode
  digitalWrite(enable, LOW);
  lcd.print("TRACKING");
}

// If more light shines on the left resistor:
if (digitalValue_left > digitalValue_right + bit_difference) {
  // Set the spinning direction clockwise:
  digitalWrite(dirPin, HIGH);
  // Increment the counter
  counter++;
  // Move the motor x number of steps
  move_stepper();
  // Update serial monitor
  serial_monitor();
  delay(50);
}

// If more light shines on the right resistor:
else if (digitalValue_left < digitalValue_right - bit_difference) {
  // Set the spinning direction counterclockwise:
  digitalWrite(dirPin, LOW);
  // Decrement the counter
  counter--;
  // Move the motor x number of steps
  move_stepper();
  // Update serial monitor
  serial_monitor();
  delay(50);
}

// This conditional checks how much light is on each photoresistor with respect to one
// another.
// If the difference is relatively small, increase the delay time between each step
if (abs(digitalValue_left - digitalValue_right) <= 10) {
  delay(15000);
  // If the difference is larger (i.e. the shadow is cast on one resistor), decrease the
  // delay time so the stepper can move more quickly
} else if (abs(digitalValue_left - digitalValue_right) > 10) {
  delay(10);
}

////////////////////////////////////// HOMING MODE ////////////////////////////////////////

} else if (digitalRead(toggle) == LOW) {

  // We don't need to induce an emergency message here because in homing mode, the user is
  // in full control of the panel's motion
  digitalWrite(enable, LOW);
  lcd.print("HOMING");

  // reset the counter to 0 and make sure to set the panel parallel to the sky
  counter = 0;
}

```

```

// The buttons only work if only one is pressed at a time
if (digitalRead(leftButton) == HIGH and digitalRead(rightButton) == LOW) {
  digitalWrite(dirPin, HIGH);
  move_stepper();
  serial_monitor();
}

if (digitalRead(leftButton) == LOW and digitalRead(rightButton) == HIGH) {
  digitalWrite(dirPin, LOW);
  move_stepper();
  serial_monitor();
}
delay(50);

}

lcd.clear();

}

//////////////////////////////// STEPPER MOTION FUNCTION //////////////////////////////////

void move_stepper() {

  for (int i = 0; i < stepsPerRevolution / 200; i++) {

    // These four lines result in 1 step:
    digitalWrite(stepPin, HIGH);
    delayMicroseconds(stepper_speed);
    digitalWrite(stepPin, LOW);
    delayMicroseconds(stepper_speed);

  }
}

//////////////////////////////// SERIAL MONITOR //////////////////////////////////

void serial_monitor() {

  Serial.print("Right:");
  Serial.print(analogRead(rightSensor));
  Serial.print(" , ");
  Serial.print("Left:");
  Serial.println(analogRead(leftSensor));
  Serial.print(" , ");
  Serial.print("Counter:");
  Serial.println(counter);
}

//////////////////////////////// EMERGENCY MESSAGE //////////////////////////////////

void emergency_message() {
  lcd.clear();
  tone(buzzer, 1000);
  digitalWrite(led, HIGH);
  delay(750);
  noTone(buzzer);
  digitalWrite(led, LOW);
  lcd.setCursor(0, 0);
  lcd.print("Please switch to");
  lcd.setCursor(0, 1);
  lcd.print("homing mode!!");
}

```

```
delay(750);
lcd.clear();
tone(buzzer, 1000);
digitalWrite(led, HIGH);
delay(750);
noTone(buzzer);
digitalWrite(led, LOW);
lcd.setCursor(0, 0);
lcd.print("Turn on the");
lcd.setCursor(0, 1);
lcd.print("serial monitor!!");
delay(750);
lcd.clear();
tone(buzzer, 1000);
digitalWrite(led, HIGH);
delay(750);
noTone(buzzer);
digitalWrite(led, LOW);
lcd.setCursor(0, 0);
lcd.print("Reconnect the");
lcd.setCursor(0, 1);
lcd.print("photoresistors");
delay(750);
}
```

## Appendix D: Battery Instructions

**How to Properly Charge the Batteries**

To properly charge your Battle Born batteries, you will want to verify that any charging component in your system is capable of being programmed for the following specifications. Charging components can include, but are not limited to converters, inverter chargers, solar charge controllers, DC to DC chargers, etc.

- Bulk/Absorption: 14.2V – 14.6V
- Absorption Time: 30 minutes per battery (for parallel string)
- Float: 13.4V – 13.8V
- Equalization: 14.4V/ Disabled
- Temperature Compensation: 0/Disabled
- Charge Rate: .5c
- Battery Charge Temperature Range: 25°F (-3°C) to 135°F (57.2°C)
- Battery Discharge Temperature Range: -4°F (-20°C) to 135°F (57.2°C)
- Cell Charge Temperature: 32°F (0°C) to 131°F (55°C)
- Cell Discharge Temperature: 68°F (20°C) to 140°F (60°C)

*NOTE: Not all chargers are capable of multistage charging. If yours is not, you will want to verify it can be programmed for the Bulk/Absorption voltage and have the other items mentioned disabled if applicable. Consult your charger's manual or the manufacturer.*

---

Battle Born Batteries BB10012 | BB10012H Manual 5

Figure D1: Instructions on How to Properly Replace the Battery (*Dragonfly Energy, 2021*)